In: Magnetic Thin Films: Properties, Performance and... ISBN: 978-1-61209-302-4
Editor: John P. Volkerts

Chapter 4

DEVELOPMENTS IN GIANT MAGNETORESISTANCE AND TUNNELING MAGNETORESISTANCE BASED SPINTRONIC DEVICES WITH PERPENDICULAR ANISOTROPY

Seongtae Bae and Naganivetha Thiyagarajah
Biomagnetics Laboratory, Department of Electrical and Computer Engineering, National University of Singapore, 117576, Singapore

INTRODUCTION

In recent years, there has been a dramatic increase in the interest towards application of giant magnetoresistance (GMR) spin-valves and magnetic tunneling junctions (MTJs) with perpendicular anisotropy in spintronics, such as a spin transfer switching (STS) magnetic random access memory (MRAM), ultra high density magnetic information devices, and low field detection spin oscillators. This interest is driven by the fact that spin-valves and MTJs with perpendicular anisotropy are expected to provide technical promises such as high thermal and magnetic stabilities that will allow the realization of extremely low dimensional and high reliability devices in more advanced spintronic applications [1-2]. In this chapter, the recent developments in GMR and tunneling magnetoresistance (TMR) spin valves and devices with perpendicular anisotropy will be reviewed and presented with distinct seven sections to understand their technical roles in advanced spintronics applications. The first section will deal with the physical origins of perpendicular anisotropy of the magnetic materials used for GMR spin-valves studied up to now. The fabrication of the magnetic thin films with perpendicular anisotropy including the optimization of film deposition conditions and the fabrication process of nano-meter sized devices will be included in this section. The GMR performance in various spin-valve structures with perpendicular anisotropy and their magnetic and thermal stabilities will also be disused in this section. The second section will focus on the physical nature of GMR and its correlation with interlayer coupling in different kinds of spin valves with perpendicular anisotropy. A newly proposed physical model of the GMR behavior interpreted in terms of the physical correlation between perpendicular anisotropy and magentostatic energy and its extension to the understanding of underlying physics of perpendicular interlayer coupling including RKKY oscillation and Néel coupling types of indirect exchange coupling will be dealt with in this section. The third section will discuss on a physical model of exchange bias and the effects of nanopatterning on the exchange bias characteristics in perpendicularly magnetized ferrimagentic/anti-ferromagentic thin films with perpendicular anisotropy for optimizing exchange biased GMR spin valves with perpendicular anisotropy. The fourth section looks at anomalous peak behavior observed in Hall effect measurements of exchange biased spin valves with perpendicular anisotropy. The fifth section will focus on magnetic tunnel junctions (MTJs) with perpendicular anisotropy. The basic theories of tunneling magnetoresistance (TMR), the initial and the recent research achievements of MTJs with perpendicular anisotropy in current spintronics will be reviewed and presented in this section. The sixth section will look at the current and potential applications of GMR and TMR devices with perpendicular anisotropy including spin-transfer switched MRAM and spin oscillator devices. The physical mechanisms and the research into the optimization of perpendicular anisotropy materials for these applications will be discussed. Finally, this chapter will be concluded with the survey on the advantages of GMR and TMR devices with perpendicular anisotropy and the future challenges targeting for the further developments in advanced spintronics applications.

1. MAGNETIC MATERIALS WITH PERPENDICULAR ANISOTROPY FOR SPIN-VALVES

This section will review perpendicular anisotropy materials considering for spin valves and the physical origin of the perpendicular anisotropy studied up to now. The fabrication of magnetic thin films with perpendicular anisotropy including the optimized deposition conditions, the fabrication process of nano-meter size devices with current-in-plane (CIP) and current-perpendicular-to-the plane (CPP) configurations as well as its structure for CIP measurement will be discussed in this section. In addition, the GMR behavior in spin-valves with perpendicular anisotropy and the magnetic and thermal stability of nano-patterned GMR spin-valves will be described in this section.

1.1. Physical Origin of Perpendicular Magnetic Anisotropy

Perpendicular magnetic anisotropy has been observed in several magnetic materials including multi-layers such as Co/Pt, Co/Pd, Co/Ni, CoFe/Pt, and CoFe/Pd, Co/Cr/Pt, alloys such as CoPt, FePt, and CoCr, and rare-earth transition metal (RE-TM) alloys such as GdFeCo, and TbFeCo [2-9]. According to the previous reports, the effective perpendicular anisotropy of these materials has been generally presented by a combination of crystalline and stress induced anisotropy expressed as Eq. (1):

$$K_{FM,\,eff} = K_{FM,\,crystalline} + K_{FM,\,stress} = (k_{u,crystalline} + 2k_{u,stress} / t_{FM}) - 2\pi M_s^2 \tag{1}$$

In the case of multi-layered thin films, both crystalline and stress-induced anisotropy contribute to generating the perpendicular anisotropy. Several studies and reviews on the origin of perpendicular anisotropy in various kinds of multi-layers combined of Co, Fe and Ni with Pd, Pt, Au, Cu and Cr have been made for the last few decades [10-15]. As the magnetic layers in these multi-layered strucutres become thinner, the contribution of surfaces and interfaces become dominant in generating the perpendicular anisotropy compared to the crystal structures (bulk properties). It has been demonstrated that smoother interface gives rise to a higher Neel surface anisotropy (interfacial perpendicular anisotropy). The interface anisotropy can be several orders of magnitude larger than magntocrystalline anisotropy and leads to aligning the net magnetization in the perpendicular direction [10]. For most of Co/X multi-layers, the perpendicular anisotropy is higher when the X is a noble metal with a larger lattice constant than Co. For example, Co/Pd (or Pt) multi-layers, the lattice mismatch was found to be more than 10 % resulting in exhibiting a high perpendicular anisotorpy. This indicates that the strain caused by lattice mismatch directly relevant to the stress-induced anisotropy contributes to the perpendicular anisotropy in these systems [11]. In addition, strong crystalline texture associated with crystalline anisotropy as well as Co-Pd or Pt mixture coherently formed at the interfaces of the multi-layered structures contributes to the perpendicular anisotropy [13].

On the other hand, ordered CoPt and FePt single layered thin films with a tetragonal $L1_0$ structure exhibit very high perpendicular magnetic anisotropy. Unlike the multi-layered [Co/Pd (Pt)] thin films, the perpendicular anisotropy in these materials is mainly due to the crystalline anisotropy. The strong magnetocrystalline anisotropy has been found to be attributed to the strong hybridization between the Pt 5-*d* band and Co or Fe 3-*d* band electronic states. Some of the key challenges for CoPt and FePt alloys were the reduction of the ordering temperature, and the control of (001) texture. A highly oriented (001) crystal structure has been achieved using MgO underlayers and thermal annealing at a temperature of 350 – 400 ^{o}C [16,17].

However, FePt has been favored for the use in ultrahigh density recording media rather than GMR spin valve materials due to its large perpendicular anisotropy of 7×10^7 erg/cm^3. While, the lower magnetization value of CoPt is favored for spin-transfer driven magnetization switching devices [18-21]. The mechanism of perpendicular anisotropy in RE-TM alloys has not yet been fully understood. RE-TM alloys exist in a mixed crystalline and amorphous state. Several mechanisms including pair ordering, columnar microstructures, single ion anisotropy, exchange anisotropy, bond-orientation anisotropy and anti-parallel dipole energies have been considered for the main physical origin of perpendicular anisotropy in these materials [22-28]. Perpendicular anisotropy, which is material and crystal strucutre dependent, has been found to be sensitive to thin film deposition conditions such as interfacial roughness, microstructures, formation of interfacial alloys and mechanical stress. Therefore, selection of suitable film growth method for special technical purpose such as MBE (Molecular Beam Epitaxial) or other evaporation techniques, sputter deposition, laser ablation deposition and electro-deposition is one of the most important factors to control the perpendicular anisotropy of the materials. Sputter deposition is more commonly used in both research and industrial applications. Higher deposition energies lead to flat multi-layers with fewer defects (dense films) however; there are more instances of inter-diffusion and stresses at the interfaces. In order to reduce these undesirable process-induced magnetic and structural degradation, sputter working parameters such as working gas pressure, input sputtering power, and inert gas are mainly controlled to adjust the stress, the roughness, the kinetic energy of sputtered atoms, and the grain size of the multi-layers. A lower sputtering kinetic energy, a higher pressure or a heavier inert gas is typically preferred to make less energetic atoms at the surface of the films. All the magnetic and non-magnetic thin films considering for spin valve multi-layers with perpendicular anisotropy can be easily controlled their magnetoelectronic and structural properties by manipulating the sputter process conditions.

1.2. Nanometer Scale Device Fabrication

Nano-meter scale patterning and device fabrication techniques are essential in determining the magnetic and thermal stability as well as in actual device realization. Electron beam lithography techniques are required to fabricate devices with nano-meter dimension. Giant magnetoresistance (GMR) with perpendicular anisotropy can be measured simply using current-in-plane (CIP) method with unpatterned films.

For simple device characterization with nanometer dimension, the device area is needed to be defined by electron beam lithography and ion-beam etching with subsequent electrode alignment and deposition on either side of the patterned device as shown in Figure 1. In CIP measurements, there is current shunting through low resistance layers thus reducing the actual resistance signal from the GMR layers. For current-perpendicular to plane (CPP) geometry, the electrodes are above and below the spin-valve or MTJ structure such that the current direction is perpendicular to the film planes. The CPP devices require well defined nano-device fabrication.

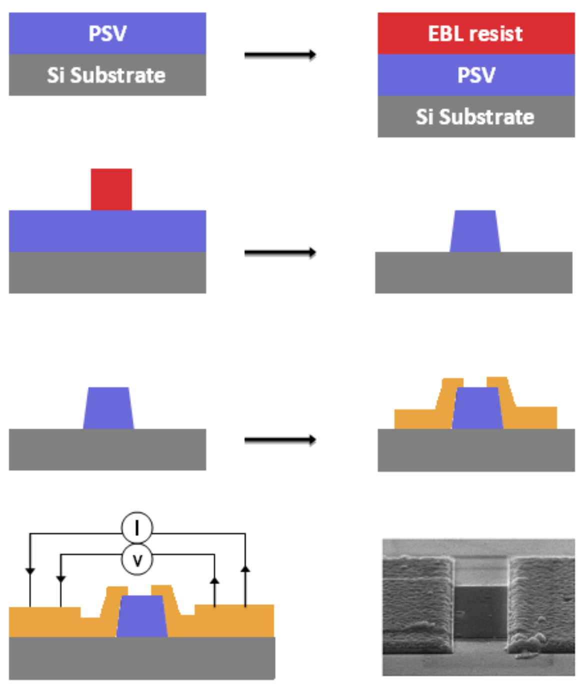

Figure 1. Fabrication process of nano-size controlled spin valves devices with perpendicular anisotropy for CIP measurement.

Generally, the CPP fabrication is based on either subtractive or additive processes. In the subtractive process, the multi-layer structure is first deposited onto the substrate. The pillar shaped structure is subsequently fabricated by masked etching steps to remove parts of the film. After depositing electrical isolation with an oxide film and etch-back or planarization process, the top electrode is deposited. A subtractive process of CPP fabrication is illustrated in Figure 2. An additive process uses a predefined structure on the substrate as a mask to define the CPP structure as illustrated in Figure 3. This process is simpler than the subtractive process in that magnetic materials have problems associated with etching. A method of defining the CPP structure without etching is potentially preferred.

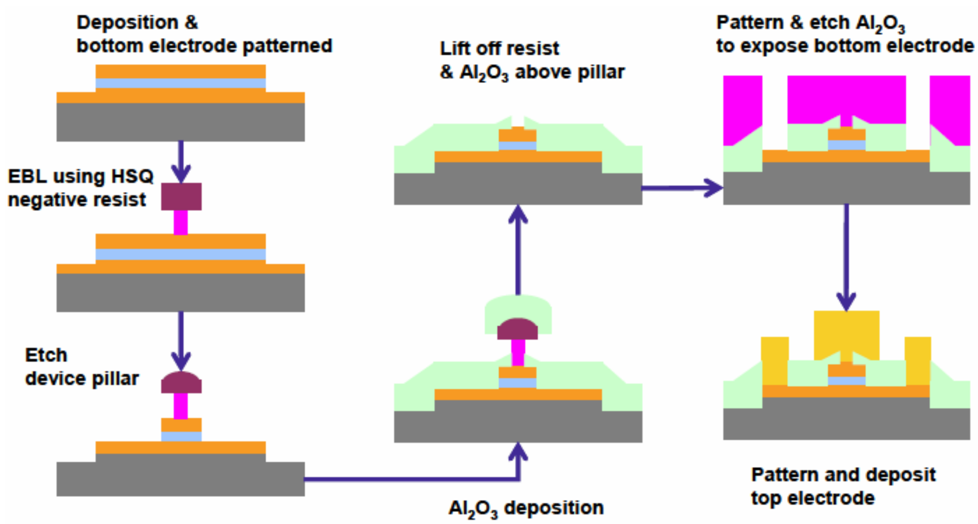

Figure 2.Current-perpendicular to plane (CPP) device fabrication (subtractive).

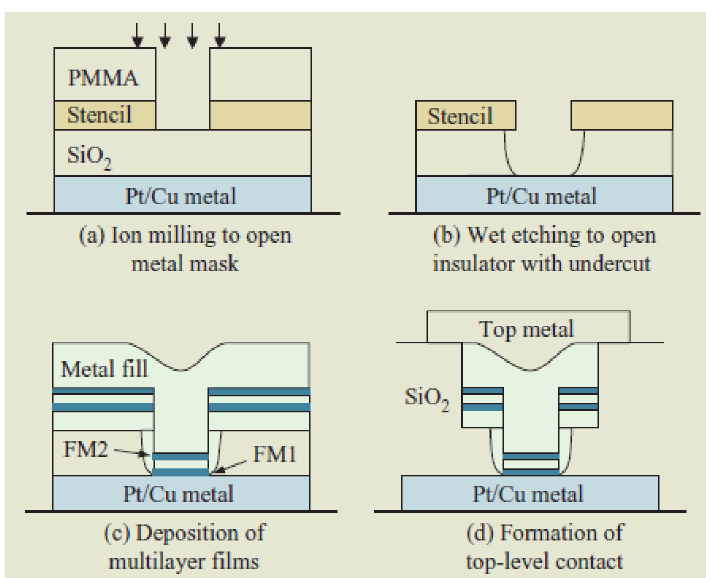

Figure 3. Current-perpendicular to plane (CPP) device fabrication (additive) [29].

1.3. GMR Behaviour in Spin-Valves with Perpendicular Anisotropy

The GMR effect originates from the spin-dependent scattering of majority and minority electrons passing through the magnetic layers. If an electron spin is parallel to the magnetization of the magnetic layers, it experiences weak scattering and hence a low resistance channel, while the electron with the opposing spin forms a high resistance channel. If the magnetic layers are anti-parallel with opposing magnetization directions, each spin direction experiences strong scattering in the magnetic layer whose magnetic moments are opposite to it. This results in a high resistance state. Based on Motts two-current model [30], the GMR phenomenon in a spin-valve system may be described as illustrated in Figure 4.

Based on the two-current model in Figure 4, the parallel and anti-parallel resistance states are given by Eq. (2).

$$R_P = \frac{R_\uparrow R_\downarrow}{R_\uparrow + R_\downarrow} \qquad R_{AP} = \frac{R_\uparrow + R_\downarrow}{2} \tag{2}$$

Accordingly, the GMR can be defined by Eq. (3),

$$GMR = \frac{R_{AP} - R_P}{R_P} = \frac{\left(R_\uparrow - R_\downarrow\right)^2}{4R_\uparrow R_\downarrow} \tag{3}$$

The GMR effects may be observed in several spin valve configurations with perpendicular anisotropy. The GMR curves of several [Co/Pd], [Co/Pt] and [Co/Ni] based pseudo spin-valves and exchange biased spin-valves presented in recent works are shown in Figures 5 ~ 8.

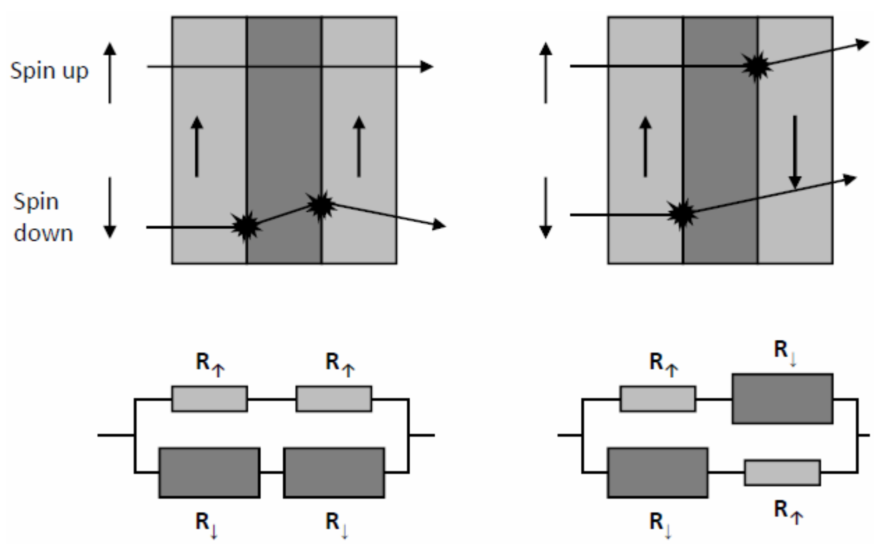

Figure 4. Two current model and equivalent resistor network showing GMR effect.

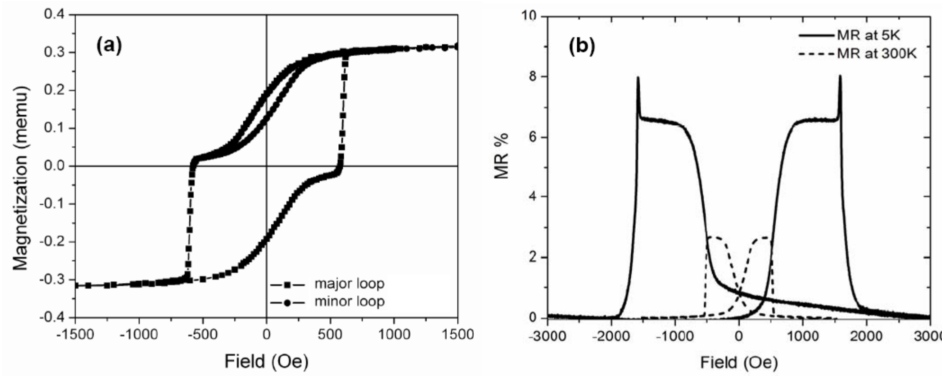

Figure 5.M-H (a) and GMR (b) curves of $[Co/Pd]_2/Cu/[Co/Pd]_4$ pseudo spin valves with perpendicular anisotropy [31].

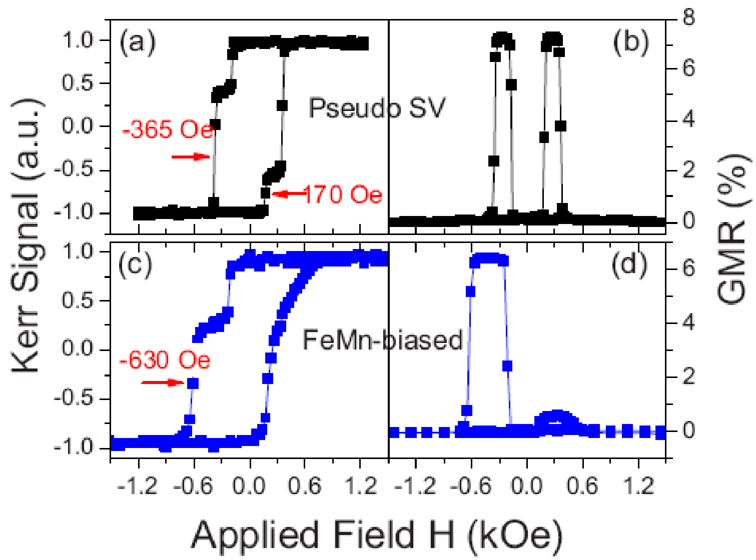

Figure 6. M-H and GMR loops of $[Co/Ni]_3/Cu/[Co/Ni]_5$ pseudo (top) and exchange biased (bottom) spin valves [32].

In a pseudo spin-valve consisting of two magnetic layers separated by a non-magnetic spacer, one of the magnetic layers is defined as a "hard layer" with a higher coercivity and the other is defined as a "soft layer" with a lower coercivity (see Figure 5 and 6). Due to the difference in coercivity, the magnetic moments of the hard and soft layers are magnetically reversed at different values of the applied magnetic field, providing a field range in which they are anti-parallel spin state (high resistance state). However, as shown in Figure 7. and 8, the exchange biased spin valve has an anti-ferromagnetic layer pinning the magnetization of one of the magnetic layers (pinned layer) by direct exchange coupling while, the other is free to rotate responded to the applied magnetic field. Due to the pinning caused by the exchange bias (shown as a hysteresis shift in hysteresis loop, (Figure 7 and 8), the free and pinned perpendicularly magnetized ferromagnetic multi-layers or single layer exhibit anti-parallel spin state leading to a high resistance state. As can be seen in Figure 7.(b), the [Co/Pd] based spin-valves exchange biased by FeMn anti-ferromagnetic layer had a GMR ratio in the range between 4 and 10 % depending on Co layer thickness. The main mechanism of GMR effect in this structure is understood in terms of spin dependent scattering at the Cu/[Co/Pd] interfaces. The strong dependence of Co layer thickness on the GMR ratio indicates that bulk scattering is another physical contribution to the magnetoresistance similar to the spin-valves with in-plane anisotropy.

Several other structures have also been introduced to improve the GMR by improving the spin-dependent scattering. One of these is a dual spin valve in which the free layer is placed between the two pinned layers to increase the number of spin-dependent scattering interfaces (or centers) for enhancing GMR performance. Figure 9. shows the GMR curve of a dual spin valve consisting of [CoFe/Pd] based free layer sandwiched between the two [Co/Pd] based hard layers with different spin-polarization ratio. This structure can be used not only for improving GMR ratio but also for the implementation of a multistate storage device because it can allow for four distinct resistance states under the externally applied switching fields.

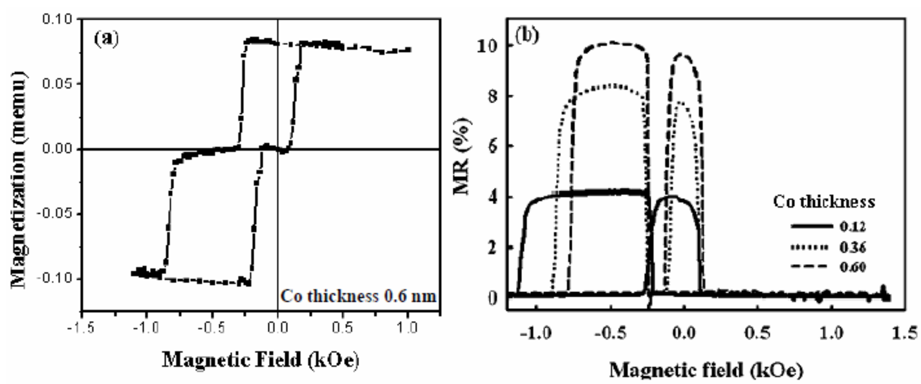

Figure 7. M-H (a) and GMR (b) curves of $[Co/Pd]_2$/Pd/Co(t)/Cu/Co/$[Co/Pd]_4$/FeMn exchange biased spin valves with perpendicular anisotropy [33]

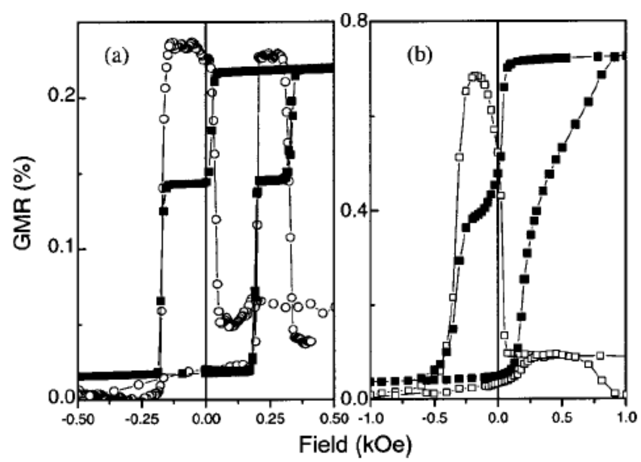

Figure 8. Extraordinary Hall effect (solid) and GMR (open) loops for $[Co/Pt]_5$/Co/Cu/Co/$[Pt/Co]_5$/ FeMn exchange biased spin valves [34].

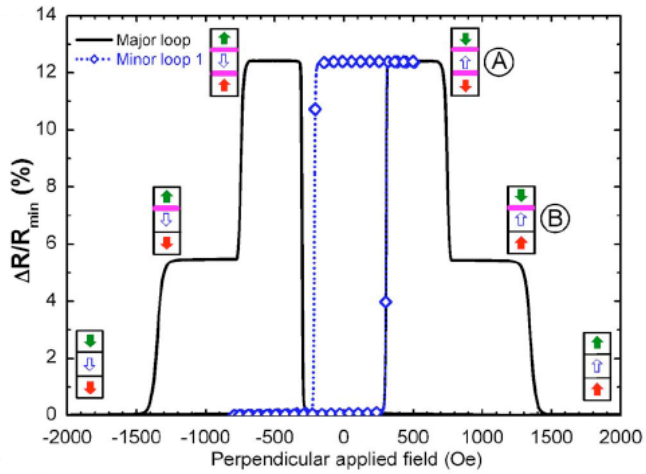

Figure 9. GMR curve of $[Co/Pd]_4/Cu/CoFe/[Pd/CoFe]_3/Cu/Co/[Pd/Co]_4$ dual pseudo spin-valve structure (minor loop in dotted line) [35].

1.4. Magnetic and Thermal Stability

One of the most important properties of perpendicular anisotropy materials is that it can be scaled down to sub-micron or even nano-meter dimensions with high magnetic and thermal stabilities. Nishimura *et al.* [1] demonstrated uniform perpendicular magnetization in 300 x 300 nm patterned GdFe/FeCo layers as shown in Figure 10. Other works [36, 37] have also demonstrated single domain magnetization in Co/Pd multilayer dot arrays.

In [38], the researchers reported on the demonstration of high magnetic and thermal stabilities in Co/Pd based spin-valves with perpendicular anisotropy. Figure 11. (a) and (b) show the GMR behavior of the nano-patterned Co/Pd based spin-valves with perpendicular anisotropy (PPSV), and NiFe/Co based spin-valves with in-plane anisotropy (IPSV), respectively.

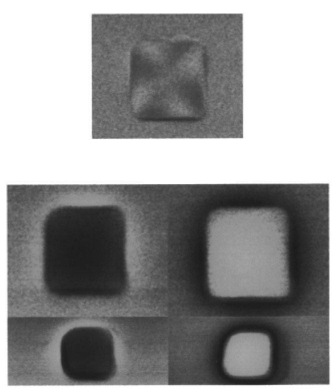

Figure 10. Magnetic-force microscopy images for the in-plane magnetization 40-nm-thick 0.5 mm x 0.5 mm square NiFe element (top) and perpendicular magnetization 100-nm-thick square GdFe/ FeCo elements; 0.5 mmx0.5 mm, and 0.3 mmx0.3 mm (bottom) at zero field [1].

As can be seen in Figure 11. (a), the GMR of the IPSV with 500 × 500 nm^2 device size was reduced by 80 % and the soft layer coercivity was increased from 12 Oe to 300 Oe (or by 2400 %). The severe increase in coercivity is due to the increased demagnetization field that results in trapped vortex magnetizations, which require larger switching fields and lead to anomalous switching behavior. They also exhibited a broad switching field characteristic, which indicates incoherent switching in the nano-patterned devices. In contrast, the PPSV with 500 × 500 nm^2 device size showed a 34 % reduction in GMR and a 16 % increase in coercivity. Further reduction down to 90 × 90 nm^2 resulted in an 82 % reduction in GMR and an 85 % increase in coercivity. As confirmed in Figure 12, the increase of coercivity is thought to be not due to the development of vortex magnetizations, but due to the possible physical damage occurring during the nano-patterning process. The reduction in GMR can be explained by device degradation resulting from the nano-patterning process as well as the geometrically induced high current density in the nano-patterned devices during measurement under constant current mode. The results shown in Figures 11. and 12 clearly demonstrate that the nano-patterned PPSV has promising magnetic and GMR switching behavior as well as electrical stability suitable for high density MRAM applications.

In order to study the thermal stability of nano-patterned IPSV and PPSV, their domain configurations were explored by MFM (Magnetic Force Microcsopy). Figure 12. shows the MFM images of the nano-patterned IPSV and PPSV with the device sizes ranging from 500 to 90 nm with an aspect ratio of 1:1. Both nano-patterned PSVs were initially saturated with a +2 kOe of magnetic field along their easy directions and then their remnant states were captured.

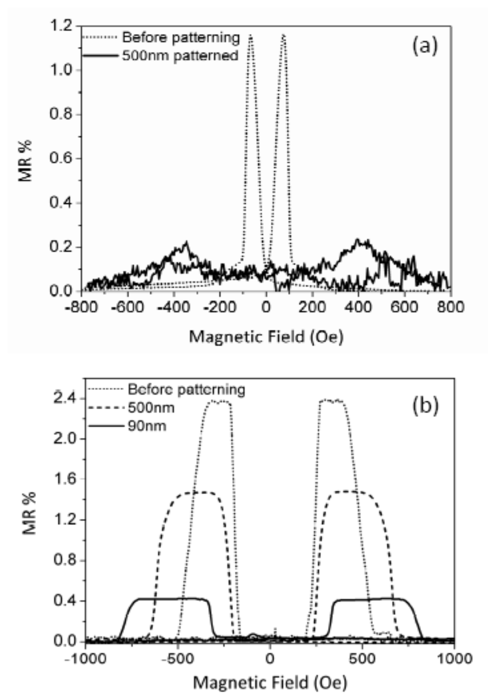

Figure 11.GMR behavior of nano-patterned (a) IPSV, (b) PPSV, and (c) PPSV measured at the different applied current densities [38].

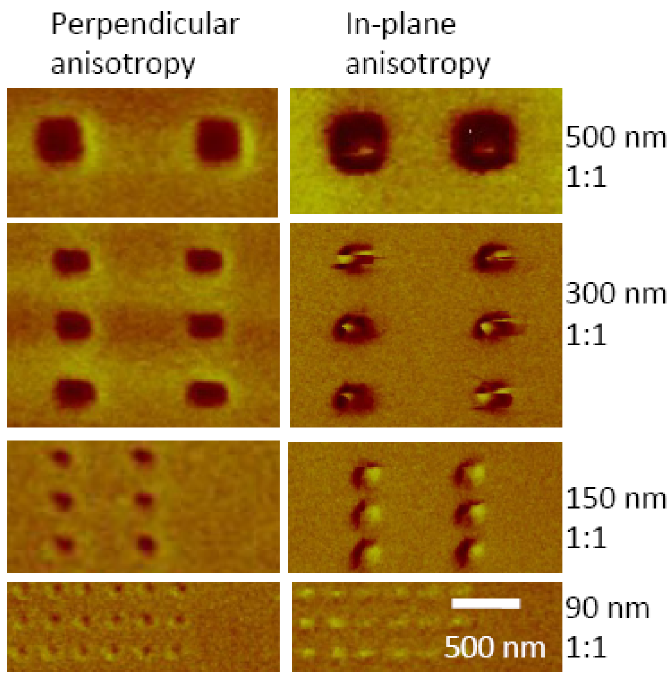

Figure 12. MFM images of nano-patterned IPSV (left) and PPSV (right) for the sizes ranging from 500 × 500 to 90 × 90 nm^2 [38].

As can be seen in Figure 12, the nano-patterned PPSV apparently show single domain structure for all the sizes ranging from 500 × 500 nm^2 down to 90 × 90 nm^2. However, the IPSVs show vortex or "flower" [39] domain structures in their remnant state. When the IPSV is patterned down to sub-micron dimensions, the devices experience curling of magnetization at the edges due to the demagnetization field, and low magnetic anisotropy resulting in the development of vortex magnetization. Thus, to maintain a single domain configuration and to remove the trapped vortices, the patterned IPSV should have a high aspect ratio above 1:5 [40] leading to a reduction in the achievable memory density particularly for MRAM applications.

2. Physical Nature of GMR and Its Correlation with Interlayer Coupling in Spin-Valves With Perpendicular Anisotropy

In order to optimize the GMR performance of the GMR spin-valves with perpendicular anisotropy for real applications in spintronics, the physical nature of GMR behavior and its correlation with interlayer coupling should be studied to precisely understand the underlying physics [41,42]. New physical models describing GMR behavior and interlayer coupling in perpendicular anisotropy systems proposed so far are reviewed and presented in this section.

2.1. A Physical Model of GMR and Interlayer Coupling Characteristics in [Co/Pd] Based Pseudo Spin-Valves with Perpendicular Anisotropy

In order to optimize GMR performance in spin-valves with perpendicular anisotropy, understanding of the physical contribution of the perpendicular interlayer coupling field to the magnetic and magnetoresistance characteristics is essentially required [43,44]. In [31,45], the physical characteristics of interlayer coupling field observed in the perpendicularly magnetized [Pd/Co]/Cu/[Co/Pd] GMR pseudo spin-valves (PSVs) were analyzed in terms of RKKY oscillation and topologically induced interlayer coupling by fitting the experimental results to the calculated values.

Figure 13. shows the dependence of Cu spacer thickness on the perpendicular interlayer coupling field and GMR behavior in Pd (3)/[Pd (1.2)/Co (0.6)]$_2$/Cu (x)/[Co (0.3)/Pd (0.6)]$_4$/Pd (3 nm) PSVs with perpendicular anisotropy. In the region of Cu thickness 1.3 and below, the two layers are strongly ferromagnetic coupled together through pinholes (or defects) and experience simultaneous switching and a correspondingly low MR. Above 1.6 nm, the soft and hard [Co/Pd] layers are ferromagnetically coupled and oscillate with a period of approximately 4.1 nm through the Cu spacer. In addition, the magnetoresistive behavior shows a strong dependence on the interlayer coupling field formed perpendicularly through the Cu spacer. The decrease of interlayer coupling field in the region of moderate interfacial roughness between 1.6 and 4.9 nm is due to the degradation of the perpendicular anisotropy in the soft layer.

Although there is a decreasing trend in the GMR probably due the shunting of current through the thicker Cu, the oscillations follow the periodic oscillation corresponding to that of the interlayer coupling field. This indicates that the GMR behavior in the PSVs with perpendicular anisotropy is dominated by the perpendicular coupling field rather than the topologically-induced magnetic coupling.

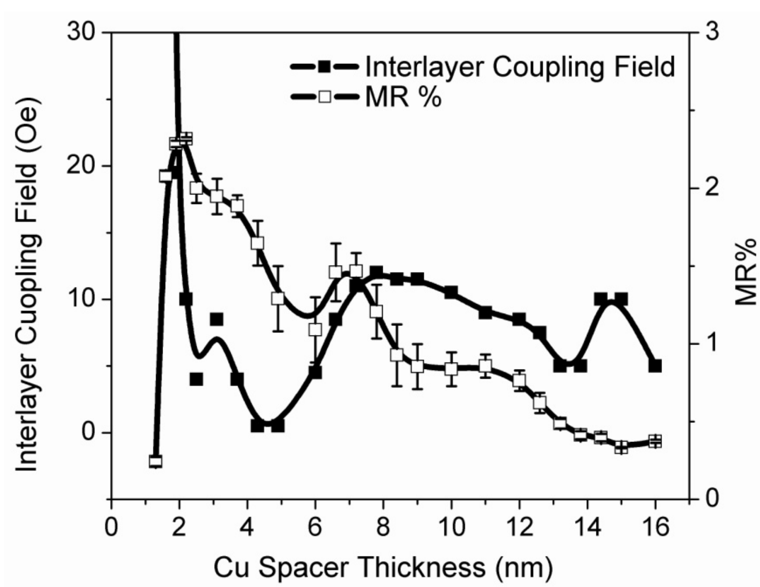

Figure 13. Dependence of interlayer coupling field and GMR ratio on the Cu spacer thickness in the Pd (3)/[Pd (1.2)/Co (0.6)]$_2$/Cu (x)/[Co (0.3)/Pd (0.6)]$_4$/Pd (3 nm) PSVs [31].

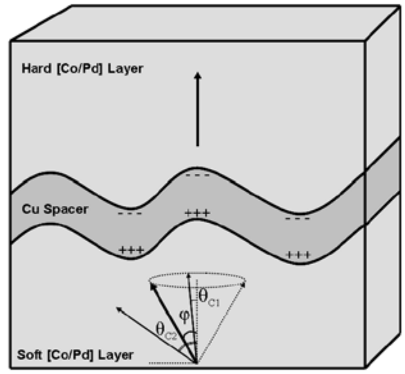

Figure 14. A schematic of Pd/$[Pd/Co]_2$/Cu/$[Co/Pd]_4$/Pd PSV structure illustrating the configurations of magnetization in the perpendicularly magnetized soft and hard [Co/Pd] multi-layers [31].

Based on these results, a new physical model for the GMR behavior in PSVs with perpendicular anisotropy has been proposed that the GMR ratio is proportional to the sine of the angle formed between the soft and hard layer magnetizations along the perpendicular direction during magnetic reversal of the soft layer by the applied magnetic field (Figure 14). Unlike the spin-valve with in-plane anisotropy, perpendicular magnetostatic field induced between the soft and hard [Co/Pd] multi-layers through the Cu spacer caused by the perpendicular anisotropy is directly relevant to the perpendicular interlayer coupling field. However, this model is only applicable once the soft [Co/Pd] multilayer magnetization is slightly tilted against the perpendicular direction. If both layers are perfectly perpendicular and strongly coupled together, they would then switch together upon the application of an external magnetic field.

2.2. Contribution of Topological and Oscillatory RKKY Coupling to the Perpendicular Interlayer Coupling

The topological coupling energy in GMR spin valves with in-plane anisotropy is expressed as Eq. (4),

$$E_{topology} = \frac{\pi}{\sqrt{2}} \frac{h^2}{\lambda} M_1 M_2 \exp\left(\frac{-2\pi\sqrt{2}t_{Cu}}{\lambda} \right) \tag{4}$$

where, h is the waviness amplitude and λ is the wavelength of the surface variations of the spin valve multi-layers, which are determined from AFM (Atomic Force Microscopy) and XTEM (cross sectional Transmission Electron Microscopy) measurements. In addition, the RKKY oscillatory coupling energy of GMR spin valves with in-plane anisotropy is expressed as Eq. (5),

$$\Delta E_{RKKY} = C \frac{m}{\hbar^2 \left(2\pi^2\right)} \frac{\sin\left(2k_F t_{Cu}\right)}{{t_{Cu}}^2} |M_1||M_2| \cos\varphi \tag{5}$$

where, $\hbar$ is the Planks constant, m is the electron mass, and k_F is wave vector at the Fermi surface and energy state **k** [46-48].

However, in the [Co/Pd] PSVs with perpendicular anisotropy, the perpendicular magnetostatic field formed between hard and soft [Co/Pd] multi-layers and spin wave generated from the [Co/Pd] soft layer physically associated with the RKKY oscillation are directly relevant to the magnetization angle of the soft layer deviated from the perpendicular direction.

Hence the general RKKY coupling formula is needed to be modified by adding a cosφ function term where the angle φ is defined as the angle between soft and hard [Co/Pd] multi-layer magnetizations. The results of the calculations shown in Figure 15. indicate that the topological coupling induced by rougher surface roughness is not dominant in determining the variations in the interlayer coupling field. While, the calculated RKKY coupling shows a good fit with the experimental results only if the effect of the soft layer magnetization angle is included. This implies that the deviation of the soft layer magnetization against the perpendicular direction, which is relevant to the perpendicular anisotropy (or perpendicular magnetostatic field formed between soft and hard [Co/Pd] layers), plays the most important role in determining the physical characteristics of interlayer coupling field in the PSV with perpendicular anisotropy.

It is also seen that the PSVs exhibiting only ferromagnetic coupling over the whole range of Cu thickness are corresponded well with previous reports with [Co/Pt] exchange biased spin-valves with perpendicular anisotropy.

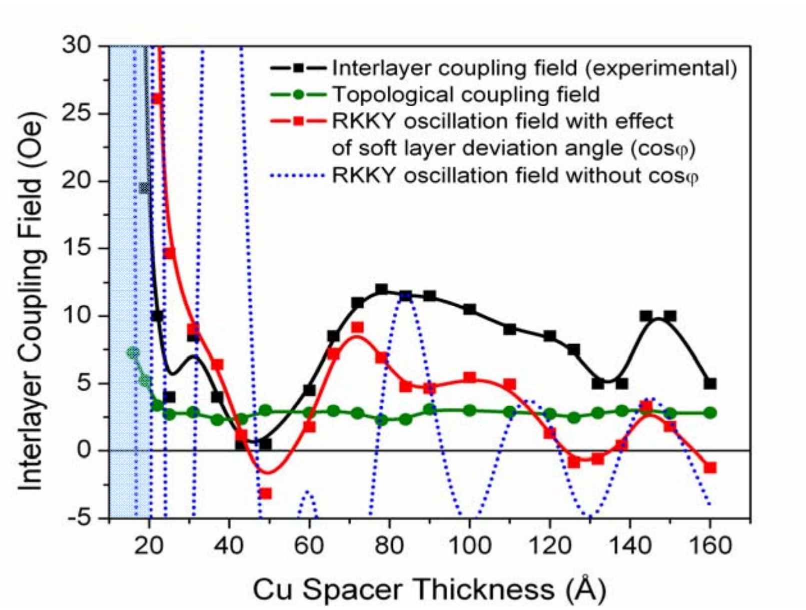

Figure 15. Dependence of experimentally observed perpendicular interlayer coupling field on the Cu spacer thickness and its physical comparison to the calculated topological coupling and oscillatory RKKY coupling fields [31].

2.3. Orange-Peel Coupling in [Co/Pt] Based Exchange Biased Spin-Valves with Perpendicular Anisotropy

Neels theory of magnetostatic coupling in magnetic multi-layers has been extended for multi-layers with perpendicular anisotropy and used to interpret the coupling in [Co/Pt] exchange biased spin-valves with Pt spacer [49].

For two ferromagnetic layers with thickness of *t* separated by a spacer with thickness *b*, the roughness of the interfaces can be described by Eq. (6),

$$z = h\cos\left(\frac{2\pi x}{T}\right) \tag{6}$$

where, 2*h* and T represent the peak-to-peak amplitude of the roughness and its wavelength. Furthermore, the local magnetizations can be described by $\psi(x) = \psi_0 \cos px$, where $p = \frac{2\pi}{T}$ and ψ_0 represents the amplitude of the magnetization fluctuations calculated by minimizing the total energy of the system according to situations of parallel and antiparallel magnetization alignments. In addition, θ is the angle difference between the normal to the interface and the z-direction (out-of-plane direction) as defined by $\theta(x) = hp\cos px$. The energy terms consist of exchange energy within each magnetic layer, anisotropy energy at each interface and magnetostatic energy. The exchange energy is given by Eq. (7),

$$E_{ex} = \frac{2t}{T}\int_0^T A\left(\frac{\partial\psi}{\partial x}\right)^2 dx = Atp^2\psi_0^2 \tag{7}$$

where, A is the exchange constant. Assuming that the anisotropy axis is always locally normal to the interface, the anisotropy energy is given by Eq. (8),

$$E_{ani} = -\frac{2t}{T}\int_0^T \cos^2\big(\theta(x) - \psi(x)\big)dx = Kt(hp - \psi_0)^2 \tag{8}$$

The magnetostatic energy eventually expressed as Eq. (9),

$$E_{mag} = \frac{\mu_0}{2}\left[-\varepsilon\frac{\sigma_1^2}{8p}\exp[-2pb]\left[1 - \exp[-2pt]^2 + \varepsilon\frac{\sigma_2^2}{4p}\exp[-p(b+t)] + \sigma_0^2 t - \frac{\sigma_1^2}{4p}\exp[-2pt]\right]\right] \tag{9}$$

where, σ_0, σ_1, and σ_2 are related to the interface density of charges σ_s, and bulk density of charges σ_v. The interface density of charges is given by Eq. (10),

$$\sigma_s = M_s\cos\left[(\theta_0 - \psi_0)\cos px\right] \approx \sigma_0 - \sigma_1\cos 2px \tag{10}$$

with $\sigma_0 = M_s\left[1 - \frac{(\theta_0 - \psi_0)^2}{4}\right]$ and $\sigma_1 = \frac{M_s}{4}(\theta_0 - \psi_0)^2$.

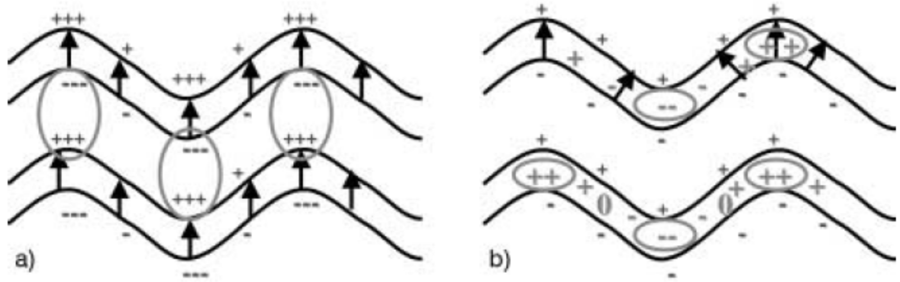

Figure 16.Schematic representation of magnetization in the case of low anisotropy (a) and high anisotropy (b) [49].

The bulk density of charges is given by $\sigma_v = \sigma_2 \sin px$ with $\sigma_2 = pM_s\psi_0 t$. The total energy is the sum of the exchange, anisotropy and the magnetostatic energies, which is then minimized with respect to ψ_0 in the parallel and anti-parallel magnetic configurations. The interlayer coupling is thus given by the difference in the total energies between the parallel and anti-parallel configurations.

The orange-peel interlayer coupling can favor either parallel or anti-parallel coupling depending on the anisotropy. In the case of a low anisotropy, the magnetization is parallel to the perpendicular direction in order to minimize surface charges and due to exchange stiffness and there are no volume charges. This leads to a dominant magnetostatic interaction between the opposite interface charge densities facing each other as shown in Figure 16.a). On the other hand, for a large anisotropy, the magnetization is aligned along the normal to the interface. For this case, the interfaces do not generate any coupling as they are uniformly charged, rather the oscillatory distribution of volume charges are out of phase for anti-parallel alignment, which is magnetostatically favorable as in Figure 16.b).

3. Physical Nature of Exchange Bias in Perpendicularly Magnetized Multi-Layers/Anti-Ferromagnetic Thin Films for GMR Spin-Valves

3.1. A Physical Model of Perpendicular Exchange Bias

Developing a physical model for a PEB system, which can clearly elucidate the underlying physics and predict what physical parameters would more effectively influence on the adjustment of the PEB characteristics has been considered to be the most urgent issue to rapidly extend the application of exchange biased GMR spin-valves with perpendicular aniosotrpy to a wider range of spintronics devices.

In [50], a physical model of PEB established based on the total energy equation per unit area of an exchange bias system by assuming coherent rotation of the magnetization is presented. This model focuses on studying the physical phenomenon of a PEB system in view of the energy competition between the anisotropy energy of AFM layer, $K_{AFM}\times t_{AFM}$, FM multi-layers, $K_{FM,eff}\times t_{FM}$ and the interfacial exchange coupling energy, J_{ex}. Unlike that of an exchange bias system with in-plane anisotropy, this model emphasizes the importance of

$K_{FM,eff} \times t_{FM}$ and the physical contribution of J_{ex} to the PEB system. The energy per unit area of an exchange bias system with in-plane anisotropy is expressed in terms of the anisotropy energy of AFM layer, $K_{AFM} \times t_{AFM}$, FM layer, $K_{FM,eff} \times t_{FM}$ and the interfacial exchange coupling energy, J_{ex}, as given by Eq. (10)[51-53],

$$E = -H_{FM} M_{FM} t_{FM} \cos(\theta - \beta) + K_{FM} t_{FM} \sin^2 \beta + K_{AFM} t_{AFM} \sin^2 \alpha - J_{INT} \cos(\beta - \alpha) \quad (11)$$

where, H is the applied field, M_{FM} the saturation magnetization, t_{FM} the thickness of FM layer, t_{AFM} the thickness of AFM layer, K_{FM} the anisotropy of FM layer, K_{AFM} the anisotropy of AFM layer and J_{INT} the interface coupling constant. By considering Eq. (11) and assuming the spin structure of AFM layer, the angles and the energy terms in a PEB system with perpendicularly magnetized FM multi-layers and AFM layer can be illustrated as shown in Figure 17. The AFM and FM anisotropy axes are assumed to be collinear and aligned in the perpendicular-to-the film direction (out of plane). As indicated in Figure 17, β, α, and θ represent the angles between the anisotropy axis and the FM magnetization, the AFM sub-lattice magnetization, and the applied field, respectively. In addition, from these viewpoints, it can be understood that the first term in Eq. (11) in a PEB system indicates the effect of the applied field on the FM multi-layers with perpendicular anisotropy, the second term is the effect of the FM anisotropy, the third term is the effect of the AFM anisotropy, and the last term accounts for the interfacial exchange coupling.

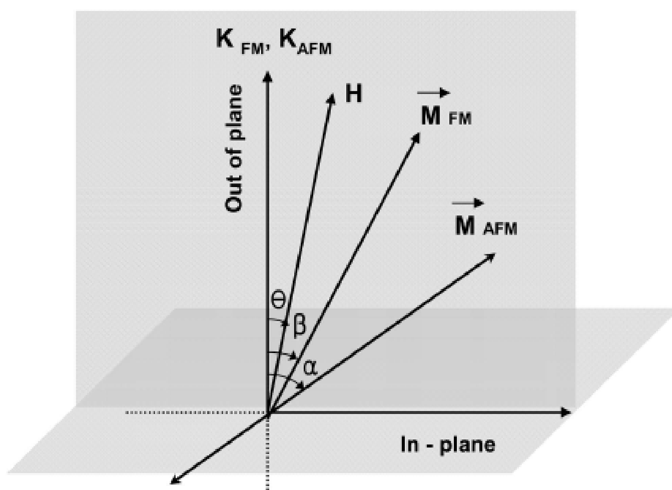

Figure 17. Schematic diagram of angles and magnetizations involved in a PEB system. The AFM and FM anisotropy axes are assumed collinear [50].

The stable state of the system can be obtained by minimizing the energy equation with respect to α and β. The energy minimization with respect to α results in Eq. (12),

$$K_{AFM} t_{AFM} \sin 2\alpha = J_{INT} \sin(\beta - \alpha) \quad (12)$$

Theoretically analyzing the result appearing in Eq. (12) clearly demonstrates that the PEB system should satisfy the critical condition of $K_{AFM} \times t_{AFM} \geq J_{INT}$ to create the exchange bias as with an exchange bias system with in-plane anisotropy. In a general energy equation for an exchange bias system (Eq. (11)), the interfacial exchange coupling energy, J_{ex}, is usually expressed as $J_{ex} = J_{INT}(\vec{S}_{FM} \bullet \vec{S}_{AFM}) = J_{INT}\cos(\beta - \alpha)$ where S_{FM} and S_{AFM} represent the spin vectors of the FM and the AFM layer. For an exchange bias system with in-plane anisotropy, J_{ex} is commonly accepted to be proportional to the cosine of angle difference between the AFM and the FM magnetization at the FM/AFM interface, because all of the spins are aligned in the in-plane direction. However, the physical nature of J_{ex} in a PEB system is different compared to an in-plane exchange bias system in that the FM and the AFM layer have two magnetization components: (1) perpendicular (out of plane) and (2) in-plane components. For a PEB system, although the angle difference between the FM and the AFM magnetizations is very small, if the spins of the FM and the AFM are not aligned in the perpendicular direction, the exchange bias field in the perpendicular direction would be kept small. Referring to Figure 17, which illustrates the magnetization of FM and AFM at the FM/AFM interface, J_{ex} of the system is understood to be proportional to the dot product of FM and AFM spin vectors.

According to the derivation as described in Eq. (13), where S_{FM} and S_{AFM} represent the spin vectors of the FM and the AFM layer, and $S_\perp$ and $S_{//}$ represent the scalar magnetization value in the perpendicular and in-plane directions, J_{ex} can be separated into two components: 1) $S_{FM\perp} \times S_{AFM\perp}$ representing the net magnetization of the FM and AFM in the perpendicular direction, which directly relates to the PEB characteristics, and 2) $S_{FM//} \times S_{AFM//}$ representing the net magnetization in the in-plane direction. For a PEB system, $S_{FM//} \times S_{AFM//}$ term is relatively negligible if the perpendicular anisotropy is strong. Therefore, in the exchange biased magnetic thin films with perpendicular anisotropy, i.e. [Pd/Co]n/FeMn PEB thin films, the interfacial exchange coupling is dominantly determined by the net magnetization of [Co/Pd]n and FeMn in the perpendicular direction; that is the cosine of the canting angle of [Co/Pd]n and FeMn magnetizations from the perpendicular direction, $J_{INT} \times (S_{[Pd/Co]_n\perp} \times S_{FeMn\perp}) = J_{INT} \times \cos\beta_{[Pd/Co]_n\perp} \times \cos\alpha_{FeMn\perp}$, as given by Eq. (14).

$$\begin{aligned} J_{ex} &= J_{INT} \times (\vec{S}_{FM} \bullet \vec{S}_{AFM}) = J_{INT} \times \cos(\beta - \alpha) \\ &= J_{INT} \times (S_{FM\perp} + S_{FM//}) \bullet (S_{AFM\perp} + S_{AFM//}) \\ &= J_{INT} \times (S_{FM\perp} \times S_{AFM\perp} + S_{FM//} \times S_{AFM//}) \end{aligned} \tag{13}$$

$$J_{ex} \approx J_{INT} \times (S_{FM\perp} \times S_{AFM\perp}) = J_{INT} \times \cos\beta_{FM} \times \cos\alpha_{AFM} \tag{14}$$

From Eq. (14), it can be seen that J_{ex} is dominated by the cosine of the canting angle of the AFM and the FM magnetizations from the perpendicular direction. In addition, Eq. (14) indicates that the improvement of the exchange bias coupling in a PEB system can be approached by enhancing the net magnetization of either AFM or perpendicularly magnetized FM layer in the perpendicular direction.

By substituting Eq. (14) into Eq. (11), the total energy equation for a PEB system can be more accurately expressed by Eq. (15), where the interfacial exchange coupling term is modified by considering the net magnetization of FM and AFM in the perpendicular direction.

$$E = -H_{FM} M_{FM} t_{FM} \cos(\theta - \beta) + K_{FM} t_{FM} \sin^2 \beta + K_{AFM} t_{AFM} \sin^2 \alpha - J_{INT} \cos \beta \cos \alpha \quad (15)$$

In order to find the exchange bias field (H_{ex}) and to explore what physical parameters significantly influence the physical characteristics of H_{ex} in a PEB system, the energy minimization of Eq. (15) with respect to β was carried out. Eq. (16) expresses the H_{ex} obtained from the energy minimization, which indicates that the net magnetization of the AFM and the FM in the perpendicular direction, relevant to cosα and cosβ, is crucial in determining the exchange bias in a PEB system. In particular, completely different from an in-plane exchange bias system, the ferromagnetic anisotropy (or anisotropy energy), K_{FM} (or $K_{AFM} \times t_{AFM}$) in a PEB system is revealed to be significant in determining the exchange bias characteristics as it directly contributes to the shift of the hysteresis loop as described in Eq. (16).

$$H_{ex} = \frac{J_{INT} \cos \alpha + 2K_{FM} t_{FM} \cos \beta}{M_{FM} t_{FM}} \quad (16)$$

A series of the experimental works using exchange biased $[Pd/Co]_5$/FeMn thin films with perpendicular anisotropy have been done to verify the physical validity of this model. In order to explore the physical contribution of $K_{AFM} \times t_{AFM}$ to the nature of PEB, two different exchange biased thin film structures with perpendicular anisotropy, Si/Ta/$[Pd/Co]_5$/FeMn/Ta and Si/Ta/FeMn/$[Pd/Co]_5$/Ta, were compared in terms of the crystalline structure (crystalline magnetic anisotropy) of FeMn AFM layer and the interfacial spin structures based on the 3Q structure model of FeMn.[54]

In addition, in order to study the physical contribution of $K_{FM,eff} \times t_{FM}$ and J_{ex} to the nature of PEB, magnetic annealing was performed at the different magnetic fields applied along the perpendicular or in-plane to the film direction [50]. All the experimental results confirmed that the proposed PEB model is valid to understand the underlying physics of PEB phenomenon in perpendicularly magnetized FM/AFM thin films.

3.2. Effect of Nano-Patterning on Exchange Bias in Perpendicularly Magnetized Multi-Layers/Anti-Ferromagnetic Structures

Studies have demonstrated that the exchange bias can be obtained in nano-patterned exchange biased perpendicularly magnetized FM/AFM thin films for ultra high density spintronics devices as shown in Figure 18. [55-57]. However, it has been undesirably found that although the patterned structures do retain their perpendicular anisotropy, the magnitude of the exchange bias field is progressively degraded and the coercivity is increased by scaling down the pattering size. For the nano-patterned exchange biased thin films, the constraints in the AFM domain size of the patterned dots imposed by the shrunken dimension dots favor and enhance the exchange bias field compared to the sheet films.

However, the reduced coordination of spins at the edges of the patterns makes them more prone to thermal activation, which supports a reduction in the exchange bias field. Furthermore, it has also been found that the blocking temperature of the system is dramatically reduced after the patterning process.

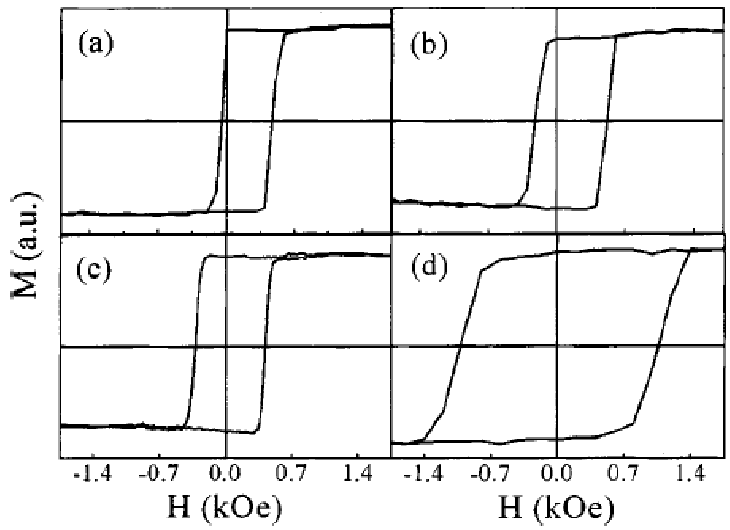

Figure 18. Hysteresis loops for [Co/Pt]/FeMn] continuous film (a), 200nm wide nanowires (b) 200 x 1000 nm stripes (c) and 200 x 200 nm dots fabricated by electron beam lithography [55].

On the other hand, it has been significant to note that in cases where the thin films were deposited on pre-patterned template showed relatively large exchange bias field compared to the post patterning with nanolithography as shown in Figure 19. The pre-patterning method avoids degradation of the process dependent material properties associated with nano-patterning processes [56]. However, as can be seen in Figure 19.a. combination of signals from the magnetic films deposited in the dots and trenches of the pre-patterned substrate has been observed in this strucure. The sharp transitions at the lower fields correspond to the magnetic reversal of the trenches, while the broader transitions at higher fields correspond to that of the dots. The broadening of the transition for the dots is attributed to the inhomogeneities among the dots leading to a larger switching field distribution.

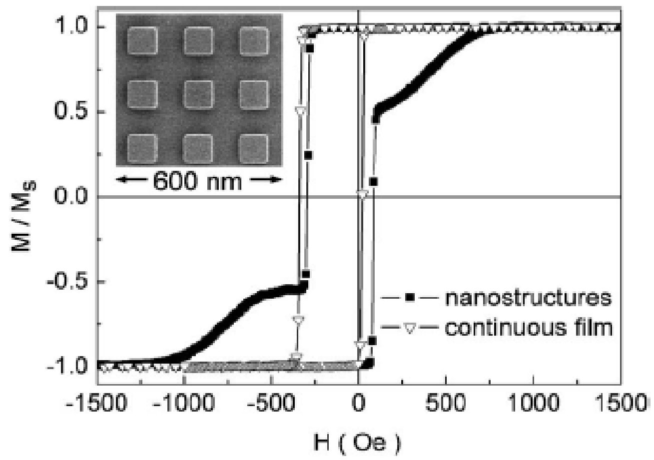

Figure 19. M-H loops of continuous and nanostructures (template of dots and trenches) of $[Pt/Co]_3/IrMn$ films with perpendicular anisotropy [56].

4. Physical Nature of Anomalous Peak Observed in Extraordinary Hall Effect Loops of Exchange Biased Spin-Valves with Perpendicular Anisotropy and Its Applications

The extraordinary Hall effect (EHE) has been widely used to measure the magnetic properties of spin-valves with perpendicular anisotropy [58-61] because the Hall resistivity is proportional to the perpendicular component of the magnetization ($M_\perp$) as shown in Eq. (17).

$$\rho_H = R_0 H + R_S M_\perp \tag{17}$$

where, H is the applied field, R_0 is the ordinary Hall coefficient and R_S is the extraordinary Hall coefficient [62]. It has been experimentally confirmed that the magnitude of the ordinary term, R_0H, is substantially small; the $R_SM_\perp$ term dominates the measured Hall signal. In recent [63], the researchers has reported on the observation of anomalous peaks in EHE loops at the switching field of the free and pinned layers, when the exchange biased [Co/Pd]/Cu/[Co/Pd]/FeMn spin-valves are magnetically reversed by an externally applied field.

Figure 19. shows the measured (a) EHE, (b) M-H, and (c) GMR loops for $Ta(20)/[Pd(0.6)/Co(0.4)]_2/$ $Cu(2.2)/Co(0.7)/[Pd(0.6)/Co(0.4)]_2/FeMn(10.8)/Ta(20$ nm). As can be seen in Figure 20, the EHE loop shows the same magnetic characteristic as the M-H and GMR measurements, with $\rho_H(H)$ being directly related to $M(H)$ as described by Eq. (17). However, the EHE loop exhibits anomalous peaks at the switching field of the free and pinned layers where the magnetization of the spin-valve is reversed by an externally applied field.

Based on the experimental results and numerical calculations, a physical model to understand anomalous peaks and their dependence on the magnetic properties of the spin-valves was proposed. For an exchange biased spin-valve, the magnetostatic energy per unit area may be defined as:

$$\begin{aligned} E = & -H_P M_S t_P \cos(\beta - \theta_P) + K_{UP} t_P \sin^2 \theta_P \\ & - M_S t_P H \cos(\alpha - \theta_P) + K_{Uf} t_f \sin^2 \theta_f \\ & - M_S t_f H \cos(\alpha - \theta_f) - J \cos(\theta_f - \theta_P) \end{aligned} \tag{18}$$

where, t_f and t_P are the free and pinned layer thickness and θ_f and θ_p are the angles between the easy axis and the free and pinned layer magnetizations respectively. M_s is the saturation magnetization of the ferromagnetic layers and K_{uf} and K_{up} are respectively the effective anisotropy constants of the free and pinned layers. H_p is the exchange biasing field, J is the interlayer coupling energy, and β is the angle between the exchange biasing field and the easy axis. H and α are the externally applied field and the angle of the applied field from the easy axis, respectively [64].

For the [Co/Pd] based exchange biased spin-valves, it can be seen that due to the large biasing field and perpendicular anisotropy constant, the total magnetostatic energy of the system is large.

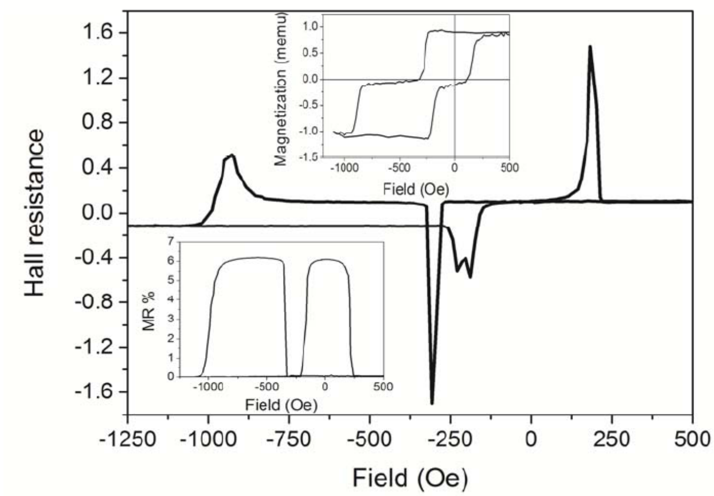

Figure 20. Observed anomalous peaks in EHE measurement and corresponding M-H and GMR measurements (inset) [63].

As an external magnetic field is applied to reverse the free or pinned layer magnetization, there is an abrupt change in the magnetostatic energy. This abrupt change is expected to lead to the appearance of the anomalous peaks in the EHE loops. The highest peak intensity across all the samples studied, is found to be the "negative free peak" which occurs as the external magnetic field is swept from a positive saturation field to negative saturation field and the free layer magnetization switches such that the spin-valve goes from a parallel state to an anti-parallel state. During this magnetization reversal of the free layer, the pinned layer magnetization would oppose the external switching field causing the magnitude of the EHE signal to increase suddenly.

In addition to the magnetostatic energy contribution to the anomalous peak, the effect of GMR on the hall resistivity is also considered. For ordinary ferromagnetic films the field dependence of ρ_H is similar to that of the magnetization M as given in Eq. (17), assuming that

R_S is field independent since the field dependence of ρ is not significant. For GMR systems, since ρ is highly field-dependant, the field dependence of R_S must be taken into account. It has been widely accepted [65,66] that extraordinary hall component is due to skew-scattering and side-jump mechanisms, where the skew-scattering contribution is proportional to ρ and both skew-scattering and side-jump mechanism contribute to the ρ^2 term [62,67] as given by Eq. (19),

$$R_S = a\rho + b\rho^2 \tag{19}$$

Taking into account the field dependence of ρ in Eq. (19), the competition between the increasing $M(H)$ and decreasing $R_S(H)$ with H also leads to the peak in the EHE measurement. The validity of the proposed model was verified by considering the physical relationship between the interlayer coupling, perpendicular anisotropy and the magnetostatic energy, as well as between the giant magnetoresistance (GMR) behavior and the Hall resistance. It was theoretically and experimentally demonstrated that the anomalous peaks provide a way of indirectly determining the magnetostatic energies, interlayer coupling behavior and GMR performance in exchange biased spin-valves with perpendicular anisotropy using EHE measurement [63].

5. Magnetic Tunneling Junctions (MTJ) With Perpendicular Anisotropy

The previous section has been primarily focused on all metal based GMR spin-valves with perpendicular anisotropy. In this section, magnetic tunneling junctions (MTJ) or tunneling magnetoressitance (TMR) with perpendicular anisotropy that has been considered and currently is being developed in spintronics research area will be discussed. This section will begin with the discussion on brief summary of tunneling magnetoresistance effects including general theory of TMR effects, physical model for spin dependent tunneling, and Simmon's theory for tunneling effects. Subsequently, the initial works on the MTJs with perpendicular anisotropy and the recent achievements of TMR spin-valves with perpendicular anisotropy in spintronic devices will be reviewed and presented.

5.1. General Theory of Tunneling Magnetoresistance Effects

Magnetic tunnel junction (MTJ) is consisted of a thin insulating layer (tunnel barrier) separated by two ferromagnetic electrodes. It exhibits tunneling magnetoresistance (TMR) due to spin-dependent electron tunneling through the barrier. The tunneling resistance when the magnetizations of the two ferromagnetic electrodes are parallel is smaller than when they are anti-parallel; this resistance change results in the TMR effect [68]. The TMR resistance change is defined as $TMR = \dfrac{R_{AP} - R_P}{R_P}$, where the P_1 and the P_2 represent spin-polarization of the ferromagnetic electrodes. The spin polarization is calculated based on the effective density of state, *D*, at the Fermi level expressed as Eq. (30),

$$P = \frac{D_{\uparrow} - D_{\downarrow}}{D_{\uparrow} + D_{\downarrow}} \tag{20}$$

and the TMR is defined in terms of the spin polarization given by Eq. (2).

$$TMR = \frac{2P_1P_2}{1 - P_1P_2} \tag{21}$$

Initial research on MTJs was based on Al-O barriers, in which various block states with different states tunnel incoherently through the amorphous barrier. However, this tunneling mechanism was found to lead to the reduction in spin-polarization and accordingly resulted in decreasing TMR ratio. A 70 % of TMR ratio has been achieved in this structure even after optimizing all the fabrication process and materials [69].

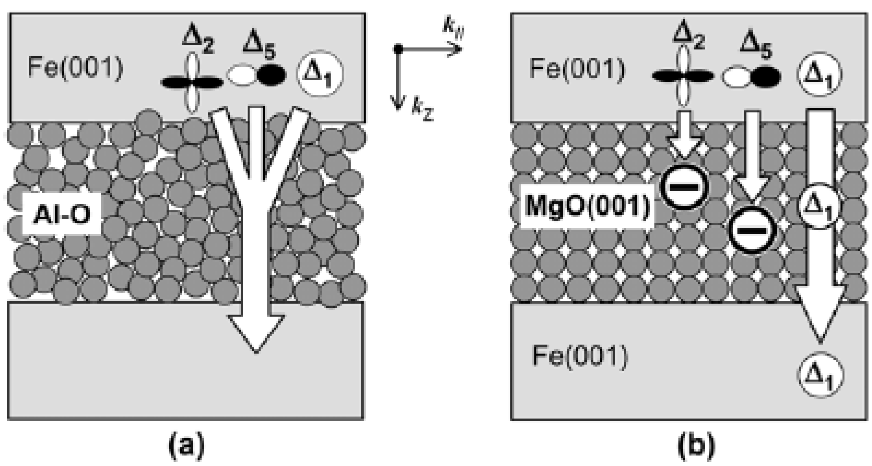

Figure 21. Schematic illustrations of electron tunneling through (a) an amorphous Al–O barrier and (b) a crystalline MgO(001) barrier [69].

More recently, an MgO (001) tunnel barrier instead of AlO_x has been attempted as a tunnel barrier and found to produce a TMR ratio over 600 % at room temperature [70]. With defect-free crystalline MgO barrier, the Block states with Δ1 symmetry dominantly tunnel through the barrier, because it acts as symmetry filter as illustrated in Figure 21.

Furthermore, MTJs with MgO tunnel barrier and ferromagnetic electrodes composed of Fe or Co and its alloys such as Fe, FeCo, CoFe, CoFeB, which are fully spin-polarized in the [001] direction at the Fermi level, have been recently revealed to exhibit a high TMR value that is preferred to advanced spintronics applications.

5.2. Model for Spin Dependent Tunneling

Spin dependent tunneling between two ferromagnetic layers depending on their relative magnetization has first reported by "Juliere" in 1975 [71]. In this model, he postulated the spin status of electrons is maintained during tunneling and the electrical conductance of spin dependent electrons is proportional to the density of states (DOS) of spin up and spin down electrons in each ferromagnetic electrode.

Based on the postulation on spin dependent tunneling, electrical conductance in metallic tunnel junction is assumed to increase when the magnetizations of two electrodes have parallel state compared to anti-parallel state. Accordingly, electrical conductance under parallel, G_p, and anti-parallel, G_{AP}, states of magnetization can be expressed by Eq. (22),

$$\begin{aligned} G_p &\propto a_1 a_2 + (1-a_1)(1-a_2) \\ G_{AP} &\propto a_1(1-a_2) + a_2(1-a_1) \end{aligned} \tag{22}$$

where, a_1 and a_2 are the relative ratio of the number of majority spin electrons in two ferromagnetic layers (or electrodes). These two parameters are expressed as $a_{1,2} = n_\uparrow/(n_\uparrow + n_\downarrow)$. From above equation, the ratio of electrical conductance depending on the relative magnetization of two ferromagnetic electrodes is defined by Eq. (23),

$$\frac{\Delta G}{G} = \frac{G_P - G_{AP}}{G_{AP}} = \frac{2P_1P_2}{1+P_1P_2} \tag{23}$$

The model of spin dependent tunneling suggested by "Julliere" is based on the "Stearns" theoretical model explaining the relationship between spin dependent tunneling current and density of state of spin electrons in metallic ferromagnet.

However, according to the experimental data reported up to now, it is revealed that this theory does not correlate well with experimental data. Different from "Julliere" model, another spin dependent tunneling model was introduced by "Slonczewski" in 1989 [72].

This model is much closer to real model in taking into account for the tunneling phenomenon in tunnel barrier separated by two ferromagnetic layers. "Slonczewski" considered wave vector, k, of electrons, which is dependent on spin states, in metallic ferromagnet and calculated wave function at the interface between metallic ferromagnetic layer and dielectric layer in terms of relative spin directions.

According to "Slonczewski" model, the relative electrical conductance depends on the damping constant of wave factor in dielectric tunnel barrier. Eq. (24) below, shows the relationship between change of conductance and damping constant of wave vector $k_\uparrow$ and $k_\downarrow$.

$$\frac{\Delta G}{G} = 2\left(\frac{k_{1\uparrow} - k_{1\downarrow}}{k_{1\uparrow} + k_{1\downarrow}}\right) \bullet \left(\frac{k^2 - k_{1\uparrow}k_{1\downarrow}}{k^2 + k_{1\uparrow}k_{1\downarrow}}\right) \bullet \left(\frac{k_{2\uparrow} - k_{2\downarrow}}{k_{2\uparrow} + k_{2\downarrow}}\right) \bullet \left(\frac{k^2 - k_{2\uparrow}k_{2\downarrow}}{k^2 + k_{2\uparrow}k_{2\downarrow}}\right) \tag{24}$$

As can be seen in the equation, the change of electrical conductance, $\Delta G/G$ is strongly dependent on the relative amplitude of damping constant of wave vectors.

5.3. Simmon's Theory for Electric Tunnel Effects

In general, there are two theories using a relationship between current and voltage characteristics in confirming electric tunnel effects in tunnel junctions separated by dielectric tunnel barriers. One is called by "Fowler-Nordheim" theory, which has been studied intensively in Metal-Oxide-Semiconductor (MOS) structures to verify tunneling mechanism. The other is called by "Simmon's Theory", which deals with tunneling theory using a relationship between tunneling current density, J and applied junction voltage, V. The "Simmon's theory" was established by John G. Simmon at the beginning of 1960's in tunneling junction structure, which is composed of two metal electrodes separated by insulating thin films [73].

Figure 22.(a) shows a schematic diagram of general barrier in insulating film between two metal electrodes. The tunneling current density, J is calculated by integrating tunneling electrons through tunnel barrier. The number of tunneling electrons is obtained by using the tunneling probability of electrons at the Fermi-level under different barrier potential heights, which are controlled by the applied junction voltage.

From the relationship between tunneling current density, J and the applied voltage, V, J can be expressed in terms of tunnel barrier height, ϕ, and tunnel barrier thickness S by Eq. (25),

$$J = J_0\{\bar{\phi}\exp(-A\bar{\phi}^{-\frac{1}{2}}) - (\bar{\phi}+eV)\exp[-A(\bar{\phi}+eV)^{\frac{1}{2}}]\} \tag{25}$$

where, $J_0 = \frac{e}{2\pi h}(\beta\Delta S)^{-2}$, h is plank constant, $A = (\frac{4\pi\beta\Delta S}{h})\sqrt{2m}$, and β is correction factor, which is independent of applied voltage, V and is expressed by Eq. (26),

$$\beta = 1 - [\frac{(eV/S)^2}{8\Delta S}]\int_0^{\Delta S = S\varphi_0/eV}[\frac{(\frac{\Delta S}{2}-x)^2 dx}{(\frac{\varphi_0}{2})^2}] = 1 - 1/24 = 23/24 \approx 0.96 \tag{26}$$

In the first above equation, $J_0\bar{\phi}\exp(-A\bar{\phi}^{\frac{-1}{2}})$ indicates the current component from electrode 1 to electrode 2 and $J_0(\bar{\phi}+eV)\exp[-A(\bar{\phi}+eV)^{\frac{1}{2}})]$ indicates the current component from electrode 2 to electrode 1. Figure 22.(b) shows pictorial illustration of current flow between two electrodes.

As shown in above eqation, the "Simmon's theory" is considered as a very useful and practical model in that it can provide crucial parameters of tunneling effects. If the mean value of barrier height,ϕ, and barrier thickness, S, are available, the tunneling current density can be easily obtained.

On the contrary, if there is a measured current-voltage characteristic plot, tunnel barrier thickness and height are numerically calculated by fitting measured data to the theoretical formula.

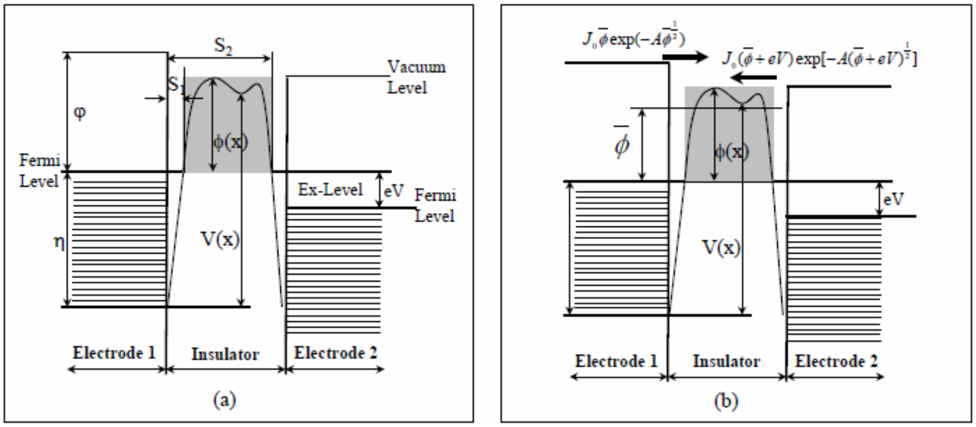

Figure 22. Schematic diagrams of (a) general barrier in insulating film between two metal electrodes, and (b) pictorial illustration of current flow between two electrodes.

5.4. Initial and Recent Works on MTJs with Perpendicular Anisotropy

With the potential advantages promised by perpendicular anisotropy materials in spintronics devices applications at an extremely low dimension, there has been an interest in the studies of MTJs with ferromagnetic electrodes with perpendicular anisotropy.

According to the first report on the TMR in a MTJ with perpendicular anisotropy in 2002, a MTJ device with RE-TM based ferromagnetic electrodes with perpendicular anisotropy and an AlO_x tunneling barrier showed more than 50 % of TMR ratio (Figure 23). In particular, this MTJ structure showed very stable TMR behavior independent of the barrier thickness as shown in Figure 23 [1].

By considering the instability of TMR performance depending on the tunnel barrier observed from the MTJs with in-plane anisotropy, the high magnetic stability as well as good thermal stability of the MTJs with perpendicular anisotropy has triggered a significant attraction to the spintronics research area. Hence, a great deal of research efforts has been intensively made for the past few years to develop various kinds of new functional MTJ systems with perpendicular anisotropy.

A variety of technical approaches in terms of materials science and physics such as using high spin polarization materials, i.e. Fe, CoFe and CoFeB with different compositions as insertion layers between the electrodes with perpendicular anisotropy and MgO tunnel barrier to improve the crystalline texture for coherent tunneling and to reduce lattice mismatch in the MgO barrier and optimizing deposition conditions of MgO tunnel barrier to make perfect (001) texture and to obtain the bulk stoichiometry of MgO have been intensively attempted as main efforts in these research scopes (Figure 24).

As a result, a 200 % of TMR ratio has been recently demonstrated in a MTJ structure with Fe based single layered ferromagnetic electrodes with perpendicular anisotropy and MgO tunneling barrier [74].

Currently, more efforts on the improvement of TMR performance and the development of high density and high speed MRAM devices using MTJs with perpendicular anisotropy are being actively made in both industry and academia for commercialization. Some of the distinct works directly relevant MTJs and MTJ based devices with perpendicular anisotropy are summarized in Table 1.

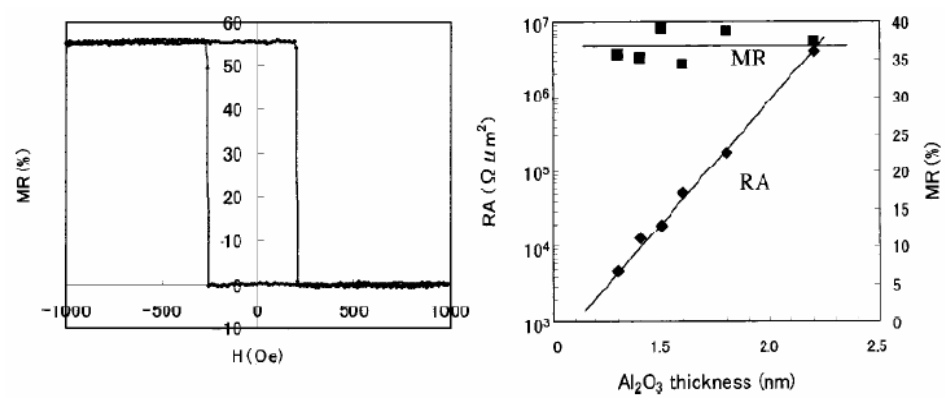

Figure 23. TMR curve of GdFe/CoFe/Al_2O_3/CoFe/TbFeCo MTJ device (left) and the dependence of junction resistance and MR as a function of barrier thickness [1].

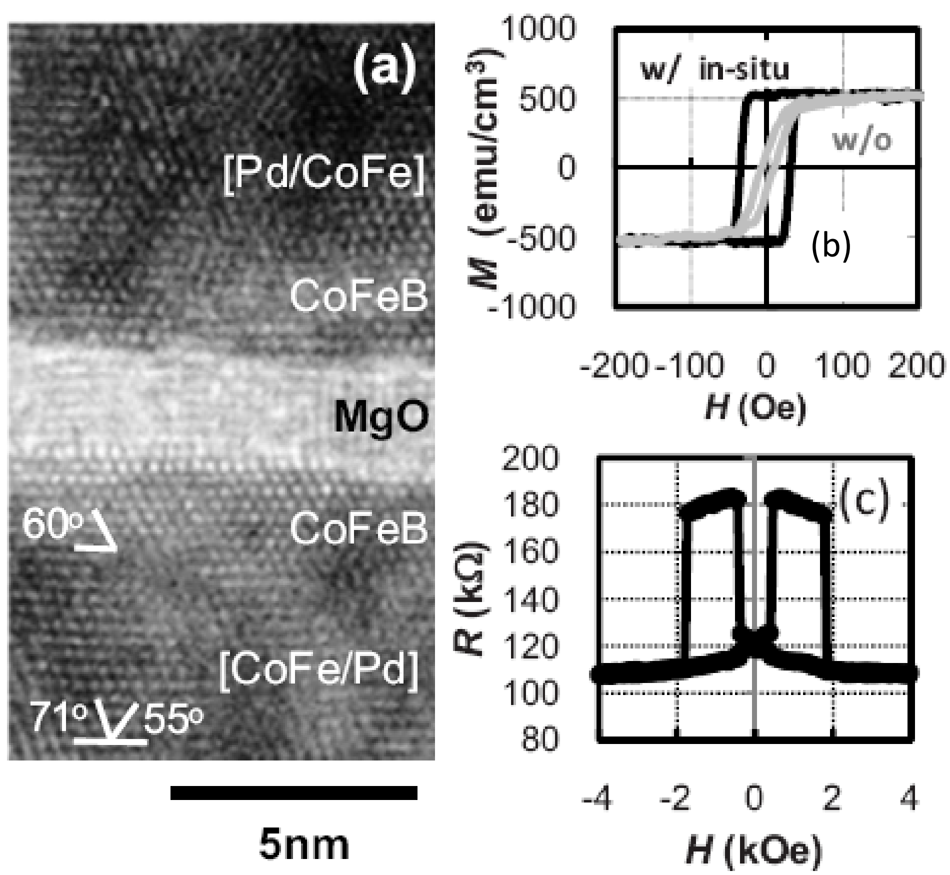

Figure 24. Cross-section TEM (a), M-H (b) and TMR (c) loops for CoFe/Pd based MTJ with MgO barrier and CoFeB insertion layers [79].

Table 1. Summary of recent MTJ works using ferromagnetic electrodes with perpendicular anisotropy

Structure	TMR ratio (%)	Remarks	Reference
$[Co/Pd$ or $Ni]_n/CoFeB/Mgo$ $/CoFeB/[Co/Pd$ or $Ni]_n$	10%	TMR not improved by annealing for CoFeB/MgO crystalization	[75]
$[Co/Pt]/AlO_x/[Co/Pt]$	14.7%	Annealing of patterned junctions increases the TMR	[76]
TbFeCo/(Mg/MgO/Mg)/GdFe Co	Not reported	Polycrystalline MgO	[77]
$Co_{90}Fe_{10}/Pd$ electrodes with CoFeB insertion, MgO barrier	1.7%	fcc(111) electrodes but imperfect MgO	[78]
with $Co_{50}Fe_{50}$	3%		
CoFe/Pd electrodes with $Co_{20}Fe_{60}B_{20}/MgO/Fe$ insertion	78%	Fe above MgO improves interface crystallinity	[79]
$Co_{60}Cr_{20}Pt_{20}/CoFe/Ru/CoFe/$ $MgO/CoFe/Ru/Co/CoCrPt$	6%		[80]
Structure	TMR ratio (%)	Remarks	Reference
$Co_{60}Cr_{20}Pt_{20}/CoFe/Ru/CoFe/$ $MgO/CoFe/Ru/Co/CoCrPt$	6%		[80]
GdFeCo/Fe/MgO/Fe/TbFeCo	64% (CIPT)	Perpendicular anisotropy by exchange coupling with RE-TM	[81]
L_{10}-FePt/MgO/L_{10}-FePt with Fe and FeCo insertion	105-120% (CIPT)	Lattice mismatch relayed by Fe insertion	[82]
[Co/Pd]/MgO/[Co/Pd]	10-12%		[83]
IrMn/Co/Pd exchange biased	8%		
L_{10}-$Co_{50}Pt_{50}/MgO/L_{10}$-$Co_{50}Pt_{50}$	6% , 13% at 10K		[84]

6. Applications of GMR and TMR Devices with Perpendicular Anisotropy

Perpendicular anisotropy materials have been widely considered for the applications in magneto-optical recording, hard-disk media and heat assisted magnetic recording media for the past few years. In more recent years, GMR spin-valve and TMR MTJ devices with perpendicular anisotropy have been intensively studied for their applications in spintronics such as a spin transfer switching MRAM due to their high magnetic stability and a lower operating current density, a spin transfer oscillator, and a spin polarized current-induced domain wall switching memory etc. The physical mechanisms of the devices and the research into the optimization of the devices are discussed in this section.

6.1. Spin Transfer Torque Magnetic Random Access Memory

As illustrated in Figure 25, when conduction electrons pass through a magnetic layer, their spins preferentially align in the direction of the magnetization of that layer (spin polarization).

As these spin polarized electrons encounter a free nano-magnetic material sandwiched between nonmagnetic spacers, the direction of their spins is repolarized to match that of the nano-magnet. This repolarization exerts a torque on the nano-magnet and as a result, its magnetic moment begins to make precession. If the current (or rate of electrons) is below a critical value, the damping torque is larger than the spin torque and the precession is quickly damped with the magnet settling into static equilibrium. If the current is well above this critical current, the spin torque is much larger than the damping torque and the precession increases in amplitude until the magnetization direction is completely reversed. This spin transfer torque exerted on a ferromagnetic layer by a sufficiently large spin polarized current, allows the manipulation of magnetization in a spin valve or magnetic tunneling junction (MTJ) into parallel (P) or anti-parallel (AP) states without the application of an external magnetic field. The AP to P transition takes place due to the spin-torque from the majority electrons polarized by the hard ferromagnetic layer while the P to AP transition takes place due to the spin-torque from the minority electrons scattered by the fixed layer.

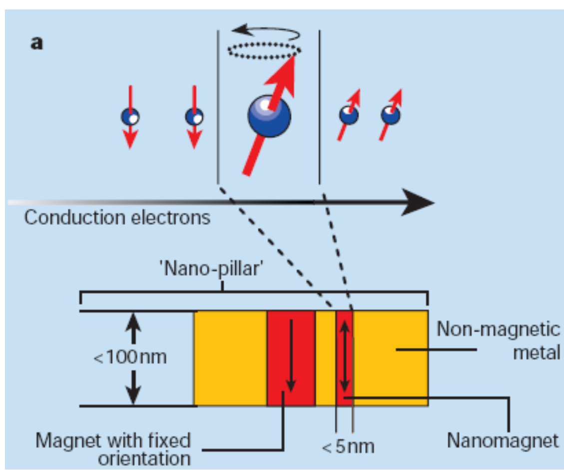

Figure 25.Spin Transfer switching mechanism [29]

Early works on spin transfer torque MRAM (See Figure 26) have been done on spin-valves and MTJs with in-plane anisotropy. However it has been theoretically anticipated that a significant enhancement and a higher thermal stability may be achieved for perpendicular anisotropy elements.

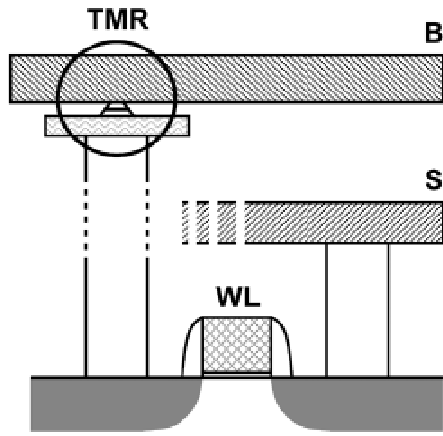

Figure 26. Illustration of spin transfer torque MRAM cell (BL: bit line, SL: source line, WL: word line) [85].

The critical reversal currents can be estimated based on Landau-Lifshitz-Gilbert (LLG) equations including spin-transfer torque term. For an in-plane anisotropy element, the critical current required for switching is given by Eq. (27).

$$I_C^{P-AP(AP-P)} \approx \frac{A\alpha M_S V}{g(0(\pi))p}(H + H_{dip} \pm H_{K\parallel} \pm 2\pi M_S) \tag{27}$$

where, M_S, V and α are the saturation magnetization, volume and Gilbert damping constant for the free layer, respectively, and p is the spin polarization of the current. H, H_{dip} and $H_{K\parallel}$ are the in-plane applied field, dipole field from the reference layer acting on the free layer and the in-plane anisotropy field, respectively.

For the spin transfer switching devices with perpendicular anisotropy, the critical currents to induce spin transfer magnetization reversal is given by Eq. (28).

$$I_C^{P-AP(AP-P)} \approx \frac{A\alpha M_S V}{g(0(\pi))p}(-H - H_{dip} \pm H_{K\perp} \mp 4\pi M_S) \tag{28}$$

It can be clearly seen that the energy barrier against thermal fluctuation is $M_S V H_K/2$ for in-plane elements and $M_S V(H_K\text{-}4\pi M_S)/2$ for perpendicular elements. This indicates that the critical current of perpendicular elements for switching is directly proportional to the anisotropy and hence the stability of the element. Since the first demonstration of spin transfer switching in full metal spin-valves using Co/Pt and Co/Ni multi-layers with perpendicular anisotropy was done in 2006 (Figure 27) [2], extensive research efforts in the development of spin-valves and MTJs with perpendicular anisotropy for the spin-transfer torque MRAM have been made [86-88] to achieve a higher density and a highly stable MRAM devices in commercialization. Table 2 shows the summary of research progress and achievements of various kinds of spin-valves and MTJ structures as well as their device performance in MRAM applications made so far.

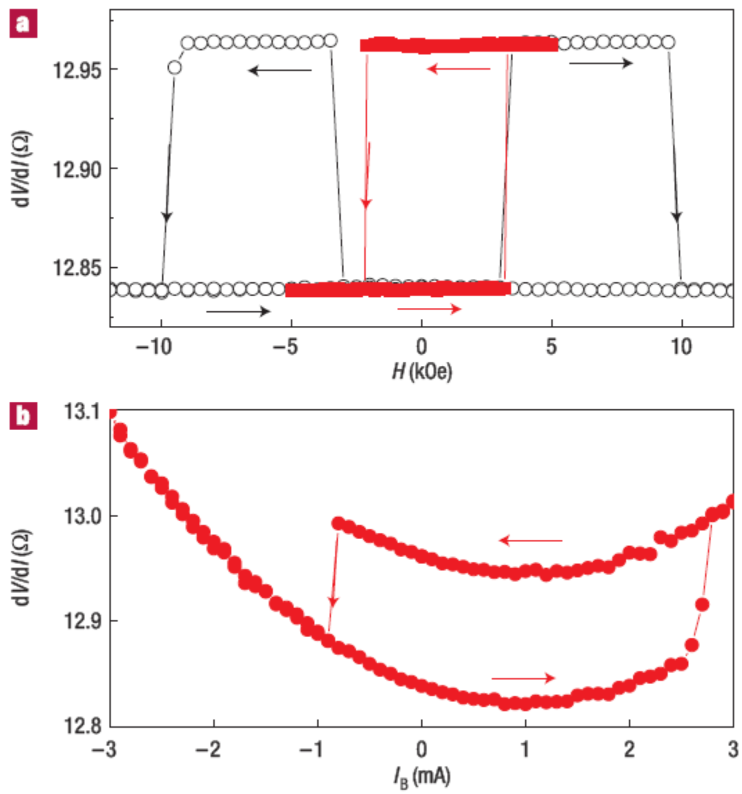

Figure 27. MR curves (solid circles represent minor loop-free layer reversal) (a) and current switching curve (b) for Co/Ni based spin-valve device with perpendicular anisotropy [2].

Table 2. Summary of spin-transfer switching device performance with perpendicular anisotropy

Structure	MR (%)	Free layer Coercivity (kOe)	Switching Current (A/cm^2) / pulse time	Reference
$[Co/Pt]_4/[Co/Ni]_2/Cu/[Co/Ni]_4$	CPP GMR 1%	2.65	P-AP: $7.5x10^7$ AP-P: $2.6x10^7$ 1000ms	[89]
$[CoFe/Pt]_5/Co/Cu/[CoFe/Pt]_7$	CPP GMR 0.47%	0.17	P-AP: 1.3 $x10^8$ AP-P: 1 $x10^8$ DC sweep	[90]
$[L1_0FePt/Au/L1_0FePt]$	CPP GMR 0.067%	5.4	AP-P: 1 $x10^8$ (6.7KOe ext. field, 77K) 100ms	[91]
TbCoFe/CoFeB/ MgO/CoFeB/TbCoFe	TMR 15%	1.2	P-AP: 4.9 $x10^6$ AP-P: 4.7 $x10^6$ 100ns	[92]
$[Co/Pt]_5/Co/[Ni/Co]_2/Co/Cu/Co/[Ni/Co]_5$	CPP GMR ~1%	0.42	P-AP,AP-P:~7 $x10^6$	[93]

$[CoFe/Pd]_3/CoFe/Cu/Co/[Pd/Co]_5$	CPP GMR 1.05	0.83	AP-P: 3.6- 3.8 x10^8 10ns	[94]
$CoFe/Cu/[CoFe/Pd]_3/CoFe/Cu/Co/ [Pd/Co]_5$	CPP GMR 0.98	0.13	AP-P: 2.9- 3.2 x10^8 10ns	
[Co/Pt]/Cu/[Co/Pt]	CPP GMR 0.33%	0.5	P-AP: 9.2 x10^7 AP-P: 6.4 x10^7	[95]
$[Co/Pt]_4/Co/[Ni/Co]_2/Cu/[Co/Ni]_2/Co$	CPP CMR 0.3%	0.245	300ps switching	[96]

6.2. Domain Wall Nucleation and Manipulation by Spin Polarized Current in GMR Devices with Perpendicular Anisotropy for Multi-State Storage

As a peculiar feature for GMR devices with perpendicular anisotropy, there have been a few of reports [97,98] of domain wall states, which have been nucleated under a spin polarized current, stabilized and manipulated in nanopillars (Figure 28).

Although this may be a drawback in current MRAM applications where care is taken to avoid domains within the magnetic layers, careful control of the domain wall creation may be of interest in development of multi-bits storage systems.

It was found that although domain wall states could be nucleated and manipulated by a spin-polarized current within a small distribution, the mechanism strongly depended on the presence of structural and magnetic imhomogenities in the device [98].

In order to utilize this phenomenon in spintronics devices, precise control of the magnetic properties of the films and the fabrication of pinning sites are essentially required.

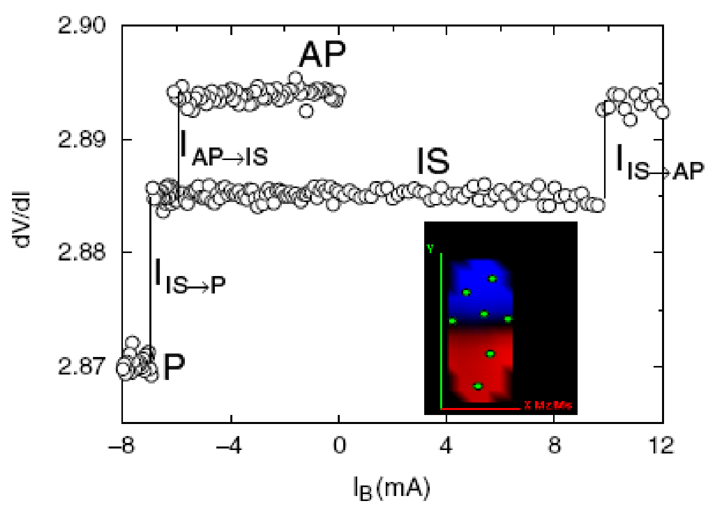

Figure 27. Differential resistance as a function of current for a 100×200 nm^2 pillar. The initial state is the AP state. The current sweeps from the AP to the IS state and then back to the AP state. The transition from the IS to P state is also shown. The inset corresponds to micromagnetic simulations (perpendicular component of the magnetization). The dots are a schematic illustration of the pinning sites. [97]

6.3. Spin Torque Oscillator

Spin transfer torque leads not only to reverse magnetization direction but also to generate high frequency precession of the magnetization. This steady-state precession corresponds to a state where the spin-transfer torque opposes and cancels the damping torque. Precession of the magnetization in spin-valves or MTJs paves the way for applications such as wide-band tunable radio-frequency oscillators [99,100]. Early spin-transfer precession was observed in systems where both the spin polarizer and free layer have an in-plane anisotropy [101]. However a more efficient system would be to have the polarizer with perpendicular anisotropy as seen in Figure 29. Polarizing the spins perpendicular to the free layer has several advantages including higher precession frequencies and lower precession currents [102].

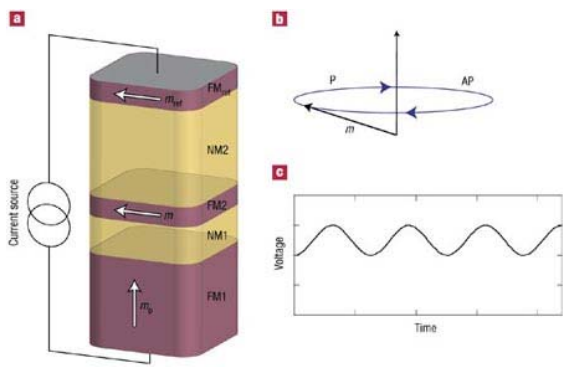

Figure 29. spin-transfer oscillator device structure with perpendicular anisotropy polarizer layer [99].

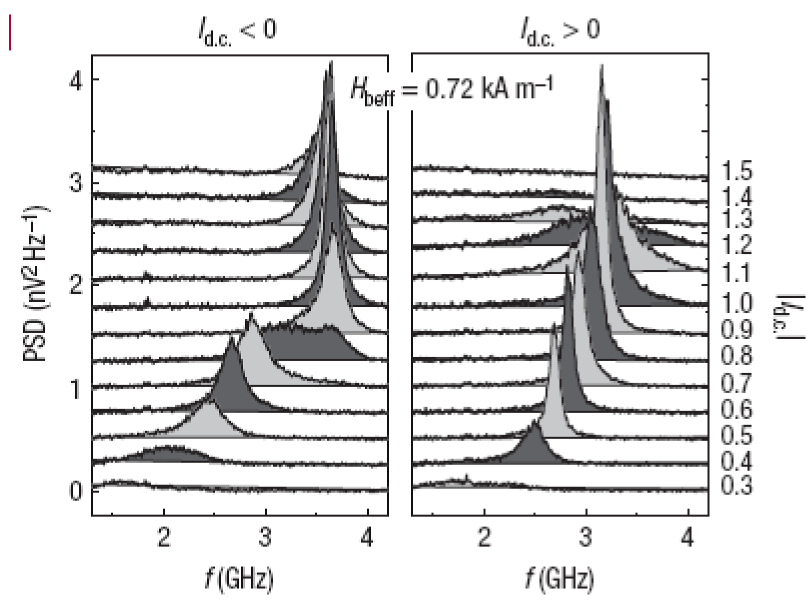

Figure 30. Power spectral density of the output voltage obtained for the spin oscillator device with perpendicular polarizer in the oscillation region for positive and negative injection currents [100]

With the perpendicular polarizer configurations, high frequency oscillations have been observed for both negative and positive injection currents as seen in Figure 30.

The spin torque oscillator provides continuous frequency tenability from zero to several gigahertz depending on the injected current. At low current densities, the oscillating frequency linearly increases with the current density. The relationship between the frequency and the injected current density is derived from the modified LLG equation as given by Eq (24)

$$f = \frac{\gamma}{2\pi\alpha}\left(\frac{P_0 \hbar J}{eM_s \delta}\right) \tag{24}$$

where, f is the oscillating frequency, J is the injected current density, M_s and δ are the saturation magnetization and thickness, respectively, P_0 denotes the polarizing faction of the spin current and α is the Gilbert damping constant [103]. As the current reaches a critical value, the frequency becomes a maximum and then the magnetization of the layers switch irreversible and the oscillations can no longer occur.

CONCLUSION AND FUTURE CHALLENGES

In this chapter, the recent developments in GMR and TMR based spintronic devices with perpendicular anisotropy have been introduced and discussed in terms materials and material process conditions, physical nature of GMR/TMR spin-valves, and the potential applications in advanced electronics. According to the literature reviews and some technical research reports published up to now, the GMR and TMR spin valves with perpendicular anisotropy have technical promises such as high magnetic and thermal stabilities for easy down sizing to a few tens of nano-meter device size, high electrical reliability due to a lower device operating current density, and easy tailoring of magnetic and structural properties by controlling process parameters. Therefore, a variety of device applications in spintronics are expected for advanced electronics such as a low current density spin transfer switching MRAM for ultra high memory density, a low current-induced domain wall switching memory, and a spin oscillator with a high spin polarizer of perpendicular component. However, despite their great technical advantages, the GMR and TMR spin valve devices with perpendicular anisotropy were found to have several technical challenges for further advanced developments in spintronics such as unbalancing of perpendicular anisotropy with shape anisotropy resulting in abrupt increase of operating current density and a larger free layer coercivity than that of GMR and TMR spin valves with in-plane anisotropy [104]. The research efforts to adjust the free layer coercivity using insertion materials such as Co, CoFe, and NiFe or use of angularly magnetized (or canted) free layers and to reduce the critical current density by increasing the spin accumulation within the GMR or TMR system such as using dual spin valves with oppositely magnetized hard layers and using spin scattering layers such as Ru, Ir and W are currently being made in this research area to overcome the technical challenges for further development.

REFERENCES

[1] N. Nishimura, T. Hirai, A Koganei, T. Ikeda, K. Okano, Y. Seguchi, and Y. Osada, *J. Appl. Phys*. 91, 5246 (2002).
[2] S. Mangin, D. Ravelosona, J. A. Katine, M.J. Carey, and E. E. Fullerton, *Nat. Mater*., 5, 210 (2006).
[3] M. Albrecht, *et. al*., *J. Appl. Phys*.,97, 103910 (2005).
[4] H. Meng *et al*., *Appl. Phys. Lett.* 88, 172506 (2006).
[5] T. Seki *et al., Appl. Phys. Lett*. 88, 172504 (2006).
[6] N. Thiyagarajah, *et al*., *Appl. Phys. Lett*. 92, 062504 (2008).
[7] P.F. Carcia, A.D. Meinhaldt, and A. Suna, *Appl. Phys. Lett*. 47, 178, (1985).
[8] T. Katayama, M. Miyazaki, Y. Nishihara and T. Shibata. *J. Magn. Magn. Mat*. 35 (1983).
[9] G. Kim, Y. Sakuraba, M. Oogane, Y. Ando, and T. Miyazaki, *Appl. Phys. Lett*. 92, 172502 (2008).
[10] M. T. Johnson, P. J. H. Bloemen, F. J. A den Broeder and J. J. de Vries, *Rep. Prog. Phys.* 59, 1409 (1996).
[11] F. J. A den Broeder, W. Hoving and P.J. H. Bloemen, *J. Magn. Magn. Mater*., 93, 562 (1991).
[12] B. N. Engel, C. D. England, R. A. Van Leeuwen, M. H. Wiedmann, and C. M. Falco, *Phys. Rev. Lett*. 67, 1910 (1991).
[13] S. Hashimoto, Y. Ochai, and K. Aso, *J. App. Phys*. 66, 4909 (1989).
[14] R. H. Victora, and J. M. MacLaren, *J. Appl. Phys*. 73, 6415 (1993).
[15] R. H. Victora, and J. M. MacLaren, *Phys. Rev*. B, 47, 11583 (1993).
[16] S. Jeong, M. E. McHenry, and D. E. Launghlin, *IEEE Trans. Magn*., 37, 1309, (2001).
[17] R. Mukai, T. Uzumaki, and A. Tanaka, *IEEE Trans. Magn*., 39, 1925, (2003).
[18] Y.-N. Hsu, S. Jeong, D. Laughlin, and D. N. Lambeth, *J. Appl. Phys*. 89, 7068.
[19] Y. F. Xu, J. S. Chen, and J. P. Wang, *Appl. Phys. Lett*. 80, 3325.
[20] K. Kang, Z. G. Zhang, C. Papusoi, and T. Suzuki, *Appl. Phys. Lett*. 84, 404.
[21] J. S. Chen, B. C. Lim, and T. J. Zhou, *J. Vac. Sci. Technol. A* 23, 184 (2005).
[22] R. J. Gambino, and J.J. Cuomo, *J. Vac. Sci. Tech.,* 15, 296 (1978).
[23] T. Mixoguchi and G. S. Cargill, *J. Appl. Phys*. 50, 3570 (1979).
[24] R. Sato, N. Saito, and Y. Togami, *Jpn. J. Appl. Phys*. 24, L266 (1985).
[25] Y. Suzuki, S. Takayama, F. Kirino, and N. Ohta, *IEEE Trans. Magn*. 23, 2275 (1987).
[26] W. H. Meiklejohn, *Proc IEEE* 74, 1570 (1986).
[27] Y. Suzuki, J. Haimovich, and T. Egami, *Phys. Rev. B* 35, 2162 (1987).
[28] H. Fu, M. Mansuripur, and P. Meystre, *Phys. Rev. B*. 66, 1086 (1991).
[29] J. Z. Sun, *IBM Res. and Dev*., 50, 81 (2006).
[30] N. F. Mott, *Proc. R. Soc. A* 153, 699, (1936).
[31] N. Thiyagarajah, and S. Bae, , *J. Appl. Phys*. 104, 113906 (2008).
[32] Z. Li, Z. Zhang, H Zhao, B. Ma, and Q. Y. Jin, *J. Appl. Phys*. 106, 013907 (2009).
[33] H. W. Joo, J. H. An, M. S. Lee, S. D. Choi, K. A. Lee, S. W. Kim, S. S. Lee, and D. G. Hwang, *J. Appl. Phys*. 99, 08R504 (2006).
[34] F. Garcia, F. Fettar, S. Auffret, B. Rodmaq and B. Dieny, *J. Appl. Phys*. 93, 8397 (2003).

[35] R. Law, R. Sbiaa, T. Liew and T.C. Chong, *J. Appl. Phys*. 105, 103911 (2009).
[36] M. Albrecht, G. Hu, A Moser, O. Hellwig, and B. D. Terris, *J. Appl. Phys*., 97, 103910 (2005).
[37] G. Hu, T. Thomson, C.T. Rettner, S. Raoux, and B. D. Terris, *J. Appl. Phys*., 97, 10J702 (2005).
[38] N. Thiyagarajah, H. W. Joo, and S. Bae, *Appl. Phys. Lett*. 95, 232513 (2009).
[39] M. E. Schabes and H. N. Bertram, *J. Appl. Phys*., 64, 1347 (1988).
[40] E. Girgis, J. Schelten, J. Shi, S. Tehrani, and H. Goronkin, *Appl. Phys. Lett*., 76, 3780 (2000).
[41] Z. Y. Liu, G. H. Yu, G. Han, and Z. C. Wang, *J. Magn. Magn. Mater*., 302, 29 (2006).
[42] Z. Y. Liu, L. Yue, D. J. Keavney, and S. Adenwalla, *Phys. Rev. B*, 70, 224423 (2004).
[43] Y. Liu, G. H. Yu, G. Han, and Z. C. Wang, *J. Magn. Magn. Mater*., 302, 29 (2006).
[44] Y. Liu, L. Yue, D. J. Keavney, and S. Adenwalla, *Phys. Rev. B,* 70, 224423 (2004).
[45] N. Thiyagarajah, S. Bae, H. W. Joo, Y. C. Han, and J. Kim, *Appl. Phys. Lett*. 92, 062504 (2008).
[46] Bruno, and C. Chappert, *Phys. Rev. Lett*., 76, 1602 (1991).
[47] Bruno, C. and Chappert, *Phys. Rev. B*, 46, 261 (1992).
[48] Coehoorn, *Phys. Rev. B*, 44, 9331 (1991).
[49] J. Moritz, F. Gacia, J. C. Toussaint, B. Dieny and J. P. Nozieres, *Europhys. Lett*. 65, 123 (2004).
[50] L. Lin, N. Thiyagarajah, H. W. Joo, J. H., K. A. Lee, and S. Bae, ., *J. Appl. Phys*., (2010).
[51] J. Nogués, and I. K. Schuller, *J. Magn. Magn. Mater*. 192, 203 (1999).
[52] H. Umebayashi, Y. Ishikawa, *J. Phys. Soc. Jpn*., 21, 1281 (1966).
[53] W. H. Meiklejohn, *J. Appl. Phys*.. 33, 1328 (1962).
[54] A. E. Berkowitz and K. Takano, *J. Magn. Magn. Mater*. 200, 552 (1999).
[55] J. Sort, B. Dieny, M. Fraune, C. Koenig, Lunnebach and G. Guntherodt, *Appl. Phys. Lett*. 84, 3696 (2004).
[56] A. Bollero, V. Baltz, B. Rodmacq, B. Dieny, and J. Sort, *Appl. Phys. Lett*. 89, 152502 (2006).
[57] J. L. Menedez, D. Ravelosona, C. Chappert, *J. Appl. Phys*. 95, 6726 (2004).
[58] C. L. Canedy, X. W. Li, and G. Xiao, *Phys. Rev. B*, 62, 508 (2000).
[59] D. Rosenblatt, M. Karpovski, and A. Gerber, *Appl. Phys. Lett*., 96, 022512 (2010).
[60] G. Xiang, A. W. Holleitner, B. L. Sheu, F. M. Mendoza, O. Maksimov, M. B. Stone, P. Schiffer, D. D. Awschalom, and N. Samarth, *Phys. Rev. B*, 71, 241307(R) (2005).
[61] D. Chiba, M. Yamaguchi, F. Matsukura, and H. Ohno, *Science*, 301, 943 (2003).
[62] C. M. Hurd, *The Hall Effect in Metals and Alloys* (Plenum, New York, 1973).N. Thiyagarajah, L. Lin, H. W. Joo, and S. Bae to be published (2010).
[63] Z. Q. Lu, G. Pan, J. Li, and W. Y. Lai, *J. Appl. Phys*., 89, 7215 (2001).
[64] A. Gerber, A. Milner, A. Finkler, M. Karpovski and L. Goldsmith, *Phys. Rev. B*, 69, 224403 (2004).
[65] Y. Yao, L. Kleinman, A. H. MacDonald, J. Sinova, T. Jungwirth, D. Wang, E. Wang, and Q. Niu, Phys. *Rev. Lett*., 92, 037204 (2004).
[66] L. Berger and G. Bergmann, in *The Hall Effect and Its Applications*, edited by C. L. Chien and C. R. Westgate (Plenum, New York, 1979).
[67] S. Yuasa and D. D. Djayaprawira, *J. Phys. D: Appl. Phys*. 40, R 337 (2007).

[68] W. D, Nordman C, Daughton J, Qian Z and Fink J *IEEE Trans. Magn.* 40 2269 (2004).
[69] Yuasa S, Fukushima A, Kubota H, Suzuki Y and Ando K , *Appl. Phys. Lett*. 89 042505 (2006).
[70] M. Julliere, *Phys. Rev. B* A84, 225 (1978).
[71] J. C. Slonczewski, *Phys. Rev. B*, 39, 1995 (1989).
[72] J. G. Simmon, *J. Appl. Phys*., 38, 2655 (1964).
[73] H. Yoda et al. 11th Joint INTERMAG MMM conference, AA-02, (2010).
[74] Z.R. Tadisina, A. Natarajarathinam, B. D. Clark, A. L. Highsmith, T. Mewes, S. Gupta, E. Chen, and S. Wang, *J. Appl. Phys*. 107, 09C703 (2010).
[75] Y. Wang, W. X. Wang, H. X. Wei, B. S. Zhang, W. S. Zhan, X. F. Han, *J. Appl. Phys*. 107, 09C711 (2010).
[76] L. X. Ye, C. M. Lee, J. H, Lai, A. Canizo-Cabrera, W. J. Chen, T. Wu, *J. Magn. Magn. Mater*. 322, L9 (2010).
[77] J.H. Park, S. Ikeda, H. Yamamoto, H. Gan, K. Mizunuma, K. Miura, H. Hasegawa, J. Hayakawa, K. Ito, F. Marsukura and H. Ohno, *IEEE Trans. Magn*. 45, 3476 (2009).
[78] K. Mizunuma, S. Ikeda, J. H. Park, H. Yamamoto, H. Gan, K. Miura, H. Hasegawa, J. Hayakawa, F. Matsukuram and H. Ohno, *Appl. Phys. Lett*., 95 232516 (2009).
[79] D. Watanabe, S. Mizukami, M. Oogane, H. Naganuma, Y. Ando, T. Miyazaki, *J. Appl. Phys.* 105, 07C911 (2009).
[80] H. Ohmori, T. Hatori, and S. Nakagawa, *J. Appl. Phys*. 103, 07A911 (2008).
[81] M. Yoshikawa, E. Kitagawa, T. Nagase, T. Daibou, M. Nagamine, K. Nishiyama, T. Kishi, H. Yoda. D. Lim, K. Kim, S. Kim, W. Y. Jeun, and S. R. Lee, *IEEE Trans. Magn*. 45, 2407 (2009).
[82] G. Kim, Y. Sakuraba, M. Oogane, Y. Ando, and T. Miyasaki, *Appl. Phys. Lett* 92, 172502 (2008).
[83] T. Kawahara, et al, *IEEE Sol. Stat. Circ*. 43, 109 (2008).
[84] H. Meng, and J. P. Wang, *Appl. Phys. Lett*. 88, 172506 (2005).
[85] T. Seki, S. Mitani, K. Yakushiji and K. Takanashi, Appl. Phys. Lett. 88, 172504 (2006).
[86] M. Yoshikawa et al, AC-01, *Intermag* (2008)
[87] S. Mangin, D. Ravelosona, J. A. Katine, M. J. Carey, B. D. Terris, and E. E. Fullerton, *Nat. Mater*. 5, 210 (2006).
[88] H. Meng, and J. P. Wang, *Appl. Phys. Lett*. 88, 172506 (2006).
[89] T. Seki, S. Mitani, K. Yakushiji and K. Takanashi, *Appl. Phys. Lett*. 88, 172504 (2006)
[90] M. Nakayama, T. Kai, N. Shimomura, M. Amano, E. Kitagawa, T. Nagase, M. Yoshikawa, T. Kishi, S. Ikegawa and H. Yoda, *J. Appl. Phys*. 103, 07A710
[91] S. Mangin, Y. Henry, D. Ravelosona, J. A. Katine, and E. E. Fullerton, *Appl. Phys. Lett*. 94, 012502.
[92] R. Law, E. Tan, R. Sbiaa, T. Liew, and T. C. Chong, *Appl. Phys. Lett*. 94, 062516 (2009).
[93] J. Park, M.T. Moneck, C. Park, J. Zhu, *J. Appl. Phys. Lett*. 105, 07D129 (2009)
[94] D. Bedau, H. Liu. J. J. Bouzaglou, A. D. Kent, J. Z. Sun, J. A. Katine, E. E. Fullerton, and S. Mangin, *Appl. Phys. Lett*. 96 022514 (2010)
[95] D. Ravelosona, S. Mangin, Y. Lemaho, J. Katine, B. Terris and E. E. Fullerton, *Phys. Rev. Lett*. 96, 186604 (2006)
[96] D. Ravelosona, S. Mangin, Y. Lemaho, J. Katine, B. Terris and E. E. Fullerton, *J. Phys. D. Appl. Phys*. 40, 1253 (2007)

[97] A. D. Kent, *Nat. Mater*., 6 399 (2007)
[98] D. Houssameddine et al., *Nat. Mater*., 6, 447 (2007)
[99] Kiselev, S. I. et al. *Nature* 425, 380–383 (2004) [102] (2004)
[100] U. Ebels, D. Houssameddine, I. Firastrau, D. Guskova, C. Thirion, B. Dieny, and L. D. Buda-Prejbeanu, *Phys. Rev. B* 78, 024436 (2008)
[101] J. A. Katine, and E.E. Fullerton, *J. Magn. Mag. Mater*. 320, 1217 (2008)